Axonal distribution of mitochondria maintains neuronal autophagy during aging via eIF2β

Kanako Shinno[1†], Yuri Miura[2], Koichi M. Iijima[3,4], Emiko Suzuki[1,5], Kanae Ando[1,6*]

1. Department of Biological Sciences, Graduate School of Science, Tokyo Metropolitan University, Hachioji, Tokyo, 192-0397, Japan
2. Research Team for Mechanism of Aging, Tokyo Metropolitan Institute for Geriatrics and Gerontology, Itabashi, Tokyo, 173-0015, Japan
3. Department of Alzheimer's Disease Research, National Center for Geriatrics and Gerontology, Obu, Aichi, 474-8511, Japan
4. Department of Experimental Gerontology, Graduate School of Pharmaceutical Sciences, Nagoya City University, Nagoya, Aichi, 467-8603, Japan
5. Gene Network Laboratory, National Institute of Genetics and Department of Genetics, SOKENDAI, Mishima, Shizuoka, 411-8540, Japan
6. Department of Biological Sciences, School of Science, Tokyo Metropolitan University, Hachioji, Tokyo, 192-0397, Japan

*Correspondence: k_ando@tmu.ac.jp

[†]Current address: Department of Neuroscience and Pathobiology, Research Institute of Environmental Medicine, Nagoya University, Chikusa-Ku, Nagoya, Aichi, 464-8601, Japan

Summary

Neuronal aging and neurodegenerative diseases are accompanied by proteostasis collapse, while cellular factors that trigger it are not identified. Impaired mitochondrial transport in the axon is another feature of aging and neurodegenerative diseases. Using *Drosophila*, we found that genetic depletion of axonal mitochondria causes dysregulation of protein degradation. Axons with mitochondrial depletion showed abnormal protein accumulation and autophagic defects. Lowering neuronal ATP levels by blocking glycolysis did not reduce autophagy, suggesting that autophagic defects are associated with mitochondrial distribution. We found that eIF2β was increased by the depletion of axonal mitochondria via proteome analysis. Phosphorylation of eIF2α, another subunit of eIF2, was lowered,

and global translation was suppressed. Neuronal overexpression of *eIF2β* phenocopied the autophagic defects and neuronal dysfunctions, and lowering *eIF2β* expression rescued those perturbations caused by depletion of axonal mitochondria. These results indicate the mitochondria-eIF2β axis maintains proteostasis in the axon, of which disruption may underly the onset and progression of age-related neurodegenerative diseases.

Highlights

- Loss of axonal mitochondria impairs autophagy and accumulates proteins in the axon
- Loss of axonal mitochondria increases eIF2β and decreases p-eIF2α
- Neuronal upregulation of eIF2β induces autophagic defects and locomotor dysfunction
- Lowering eIF2β rescues autophagic defects caused by loss of axonal mitochondria

Keywords

Mitochondria; axonal transport; aging; neuronal proteostasis; protein aggregation; autophagy; eukaryotic Initiation Factor 2β (eIF2β); *Drosophila*; neurodegeneration; proteome

Introduction

Neurons have a morphologically complex architecture composed of microcompartments and require tight regulation of the abundance of proteins and organelles spatially and temporally[1]. Such control of protein amounts, or proteostasis, is essential for neuronal functions[2] and is achieved through the orchestration of protein expression, folding, trafficking, and degradation controlled by intrinsic and environmental signals[3]. Translation is initiated by the eukaryotic initiation factor 2 (eIF2) complex[4]. eIF2, a heterotrimer of α, β, and γ subunits, transports Met-tRNA to the ribosome in a GTP-dependent manner[5]. Under stressed conditions, phosphorylation of eIF2α attenuates global translation and initiates translation of mRNAs related to the integrated stress response (ISR)[6]. As for protein degradation, autophagy and proteasome are major systems that maintain proteostasis[7]. The proteasome degrades unnecessary proteins, followed by regulated ubiquitination processes[8], and autophagy removes damaged or harmful

components, including large protein aggregates and organelles, through catabolism (selective autophagy)[9]. In addition to autophagy induced by acute stressors, a basal level of selective autophagy mediates the global turnover of damaged proteins[10].

Such constitutive autophagy decreases during aging, which may underlie declines in the structural and functional integrity of neurons[11]. Decreased protein degradation and accumulation of abnormal proteins also contribute to increased risks of neurodegenerative diseases. Age-related neurodegenerative diseases such as Alzheimer's disease and Parkinson's disease are often associated with the accumulation of misfolded proteins such as amyloid-β, tau, and α-synuclein[12]. Enhancement of autophagy mitigates age-related dysfunctions and neurodegeneration caused by proteotoxic stress[13]. However, it is not fully understood how aging disrupts the regulation of this constitutive autophagy.

Neurons are also highly energy-demanding cells. At nerve terminals, action potentials trigger the release of neurotransmitters via exocytosis of synaptic vesicles, which requires a constant supply of ATP and calcium buffering[14]. Such neuronal activity relies on mitochondrial functions[15], and mitochondria are actively transported from their major sites of biogenesis in soma to axons[16]. However, the axonal transport of mitochondria declines during aging[17,18,19]. Reduced axonal transport of mitochondria is thought to contribute to age-related declines in neuronal functions[17,19,20,21]. The number of functional mitochondria in synapses is reduced in the brains of patients suffering from age-related neurodegenerative diseases such as Alzheimer's disease[22], and mutations in genes involved in mitochondrial dynamics are linked to neurodegenerative diseases[23]. The mislocalization of mitochondria is sufficient to cause age-dependent neurodegeneration in *Drosophila* and mice[24,25], indicating that the proper distribution of mitochondria is essential to maintain neuronal functions. Thus, depletion of functional mitochondria from axons and proteostasis collapse are common features of aging and neurodegenerative diseases.

Mitochondrial transport is regulated by a series of molecular adaptors that mediate the attachment of mitochondria to molecular motors[16]. In *Drosophila*, mitochondrial transport is mediated by milton and Miro, which attaches mitochondria to microtubules via kinesin heavy chain[26,27]. In the absence of milton or Miro, synaptic terminals and axons lack mitochondria, although mitochondria are numerous in the neuronal cell body[28]. We previously reported that RNAi-mediated knockdown of *milton* or *Miro* in neurons causes a reduction in axonal mitochondria, age-dependent locomotor defects[29], and age-

107 dependent neurodegeneration in neuropile area starting around 30 days after eclosion
108 (day-old)[24], and enhances axon degeneration caused by human tau proteins[24], suggesting
109 that these flies can be used as a model to analyze the effect of depletion of axonal
110 mitochondria during aging. In this study, we investigated a causal relationship between
111 mitochondrial distribution and neuronal proteostasis by using neuronal knockdown of
112 *milton*. We found that depletion of axonal mitochondria reduced autophagy and increased
113 the accumulation of aggregated proteins in the axon prior to gross neurodegeneration.
114 Proteome analysis and follow-up biochemical analyses revealed that neuronal
115 knockdown of *milton* increased eIF2β levels and lowered phosphorylation of eIF2αin the
116 axon. In addition, *milton* knockdown suppressed global translation. Overexpression of
117 *eIF2β* was sufficient to decrease autophagy and induce neuronal dysfunction, and genetic
118 suppression of *eIF2β* restored autophagy and improved neuronal function in the *milton*
119 knockdown background. These findings suggest that loss of axonal mitochondria and
120 elevated levels of eIF2β mediate proteostasis collapse and neuronal dysfunction during
121 aging.
122
123
124 **Results**
125
126 **Depletion of axonal mitochondria by knockdown of *milton* or *Miro* causes protein**
127 **accumulation in the axon**
128 In *Drosophila*, mitochondrial transport is mediated by milton and Miro, which attach
129 mitochondria to microtubules via kinesin heavy chain[26,27] (Figure 1A). It has been
130 reported that expression of *milton* RNAi in neurons via pan-neuronal elav-GAL4 driver
131 reduced milton protein levels in *Drosophila* head lysate to 40% and mito-GFP signals in
132 axons to 50%[24,29].
133 To test how loss of axonal mitochondria affects proteostasis in neurons, we first examined
134 the accumulation of ubiquitinated proteins. At 14 day-old, more ubiquitinated proteins
135 were deposited in the brains of *milton* knockdown flies than in those of age-matched
136 control flies (Figure 1B, $p < 0.005$ between control RNAi and *milton* RNAi). There was
137 no significant increase in ubiquitinated proteins in *milton* knockdown flies at 1-day old,
138 suggesting that the accumulation of ubiquitinated proteins caused by *milton* knockdown
139 is age-dependent (Figure S1). We also analyzed the effect of the neuronal knockdown of
140 *Miro*, a partner of milton, on the accumulation of ubiquitin-positive proteins. Since severe
141 knockdown of *Miro* in neurons causes lethality, we used UAS-*Miro* RNAi strain with low
142 knockdown efficiency, whose expression driven by elav-GAL4 caused 30% reduction of

143 *Miro* mRNA in head extract[24]. Although there was a tendency for increased ubiquitin-
144 positive puncta in *Miro* knockdown brains, the difference was not significant (Figure 1B,
145 $p>0.05$ between control RNAi and *Miro* RNAi). These data suggest that the depletion of
146 axonal mitochondria induced by *milton* knockdown leads to the accumulation of
147 ubiquitinated proteins before neurodegeneration occurs.
148 It has been reported that ubiquitinated proteins accumulate with aging[30]; thus, we
149 analyzed the accumulation of ubiquitinated proteins in aged brains (30 day-old) with
150 *milton* knockdown. The number of puncta of ubiquitinated proteins did not significantly
151 differ between control and *milton* knockdown flies or between control and *Miro*
152 knockdown flies (Figure 1C, $p > 0.05$). These results suggest that depletion of axonal
153 mitochondria may have more impact on proteostasis in young neurons than in old neurons.
154 We examined the ultrastructure of presynaptic terminals and cell bodies in photoreceptor
155 neurons with *milton* knockdown by transmission electron microscopy in 27-day-old flies
156 (Figure 1D). As previously reported[24], the number of mitochondria in presynaptic
157 terminals decreased in *milton* knockdown (Figure 1E). The swelling of presynaptic
158 terminals, characterized by the enlargement and roundness, was not reported at 3-day-
159 old[24] but observed at this age with about 4% of total presynaptic terminals (Figure 1F,
160 asterisks).
161 Some presynaptic terminals of *milton* knockdown neurons contained dense materials
162 (Figure 1F and G, arrowheads). Dense materials are rarely found in age-matched control
163 neurons, indicating that *milton* knockdown induces abnormal protein accumulation in the
164 presynaptic terminals (Figure 1G and H). In *milton* knockdown neurons, dense materials
165 are found in swollen presynaptic terminals more often than in presynaptic terminals
166 without swelling, suggesting a positive correlation between the disruption of proteostasis
167 and axonal damage (Figure 1G). In contrast, dense materials were not observed in cell
168 bodies in the *milton* knockdown retina (Figure 1H). These results indicate that the
169 depletion of axonal mitochondria induces protein accumulation in the axon.
170
171 **Depletion of axonal mitochondria impairs protein degradation pathways**
172 Since abnormal proteins were accumulated in *milton* knockdown brains, we next
173 examined if protein degradation pathways were suppressed. We analyzed autophagy via
174 western blotting of the autophagy markers LC3 and p62[31]. During autophagy progression,
175 LC3 is conjugated with phosphatidylethanolamine to form LC3-II, which localizes to
176 isolation membranes and autophagosomes. LC3-I accumulation occurs when
177 autophagosome formation is impaired, and LC3-II accumulation is associated with
178 lysosomal defects[31,32]. p62 is an autophagy substrate, and its accumulation suggests

179 autophagic defects[31,32]. We found that *milton* knockdown increased LC3-I, and the LC3-
180 II/LC3-I ratio was lower in *milton* knockdown flies than in control flies at 14-day-old
181 (Figure 2A). We also analyzed p62 levels in head lysates sequentially extracted using
182 detergents with different stringencies (1% Triton X-100 and 2% SDS). Western blotting
183 revealed that p62 levels were increased in the brains of 14-day-old of *milton* knockdown
184 flies (Figure 2B). The increase in the p62 level was significant in the Triton X-100-soluble
185 fraction but not in the SDS-soluble fraction (Figure 2B), suggesting that depletion of
186 axonal mitochondria impairs the degradation of less-aggregated proteins. Proteasome
187 activity was also significantly decreased in brains with neuronal knockdown of *milton*
188 (Figure 2C, $p < 0.005$).
189 At 30 day-old, LC3-I was still higher, and the LC3-II/LC3-I ratio was lower, in *milton*
190 knockdown compared to the control (Figure 2D). At this age, *milton* knockdown
191 increased p62 significantly in 1% Triton X-100 fraction and 2% SDS fraction (Figure 2E).
192 Proteasome activities were also decreased in *milton* knockdown flies at 30-day-old
193 (Figure 2F). These results indicate that depletion of axonal mitochondria impairs protein
194 degradation pathways.
195
196 **ATP deprivation does not impair autophagy**
197 *milton* knockdown downregulates ATP in the axon[33]. To examine whether the disruption
198 of protein degradation pathways by *milton* knockdown is due to ATP deprivation, we
199 investigated the effects of knocking down phosphofructokinase (*Pfk*), a rate-limiting
200 enzyme in glycolysis, on protein degradation pathways. Neuronal knockdown of *Pfk* was
201 reported to lower ATP levels in brain neurons[33]. *Pfk* knockdown and *milton* knockdown
202 decreased ATP to similar levels (Figure 3A-C). However, in contrast with *milton*
203 knockdown, *Pfk* knockdown did not affect the levels of LC3-I, LC3-II or the LC3-II/LC3-
204 I ratio (Figure 3D). *Pfk* knockdown decreased p62 level (Figure 3E), suggesting that
205 autophagy is promoted. On the other hand, proteasome activity was decreased by *Pfk*
206 knockdown (Figure 3F). These results suggest that the downregulation of axonal ATP
207 upon depletion of axonal mitochondria decreases proteasome activity, but not autophagy.
208
209 **Proteome analysis suggests that depletion of axonal mitochondria causes disruption**
210 **of autophagy and premature aging**
211 To identify the pathways that mediate the decrease in autophagy in *milton* knockdown
212 brains, we performed proteome analysis to systematically detect differentially expressed
213 proteins upon neuronal knockdown of *milton*. We analyzed flies at 7- and 21-day-old, the
214 age before autophagic defects are detected and the age just before the onset of

215 neurodegeneration, respectively (Figure 4A). 1039 proteins were detected by liquid
216 chromatography-tandem mass spectrometry (LC-MS/MS). Expression of 36 proteins was
217 significantly increased (22 proteins) or decreased (14 proteins) by *milton* knockdown at
218 7-day-old (Figure 4B, Tables 1 and S1). At 21 day-old, the expression of 41 proteins (31
219 upregulated and ten downregulated proteins) was significantly altered in *milton*
220 knockdown flies compared with control flies (Figure 4C, Tables 1 and S1). The
221 "Interaction search" algorithm using KeyMolnet showed that proteins whose expression
222 was significantly altered in the brains of *milton* knockdown flies at both 7- and 21-day-
223 old were closely associated with the autophagic pathway (Table 2). Proteins involved in
224 pathways characteristics of aging, such as the immune response (Transcriptional
225 regulation by STAT), cancer (Transcriptional regulation by SMAD, Transcriptional
226 regulation by myc), longevity (Transcriptional regulation by FOXO, Sirtuin signaling
227 pathway), and stress responses (HSP90 signaling pathway, MAPK signaling pathway)[34,35],
228 were enriched in the proteome profiles of *milton* knockdown flies compared with those
229 of control flies at 7-day-old (Table 2), suggesting that depletion of axonal mitochondria
230 accelerates aging in the brain.
231
232 **Depletion of axonal mitochondria upregulates eIF2β and decreases phosphorylation**
233 **of eIF2α**
234 Differentially expressed proteins at 7-day-old flies may reflect alterations that are causal
235 for autophagic defects. We noticed that the expression level of eIF2β was 2.465-fold
236 higher in the brains of *milton* knockdown flies than in those of control flies (Figure 4B
237 and D). Upregulation of eIF2β in the brains of *milton* knockdown flies was confirmed by
238 western blotting. *milton* knockdown increased eIF2β protein levels more than twice
239 (Figure 4E), but did not change the level of *eIF2β* mRNA (Figure 4F).
240 eIF2β is a subunit of the eukaryotic initiation factor 2 (eIF2) complex, which is critical
241 for translation initiation and the integrated stress response (ISR)[4]. eIF2 is a heterotrimer
242 of α, β, and γ subunits, and eIF2α is phosphorylated during the ISR[6]. As for the other
243 subunits of eIF2 complex, proteome analysis did not detect a significant difference in the
244 protein levels of eIF2α and eIF2γ between *milton* knockdown and control flies at 7 and
245 21 days (Figure 4D). Western blotting of brain lysates showed that *milton* knockdown
246 reduced eIF2α levels (Figure 4G), while p-eIF2α levels were not significantly affected
247 (Figure 4H).
248 To analyze local changes of eIF2α and p-eIF2α, we carried out immunostaining. We
249 focused on the mushroom body, where axons, dendrites, and cell bodies can be easily
250 identified (Figure 4I). Both eIF2α and p-eIF2α were downregulated in the cell body

251 (Kenyon cells) and dendritic (Calyxes) regions of the brains of *milton* knockdown flies
252 (Figure 4J). In axons (lobe tips), *milton* knockdown did not affect eIF2α (Figure 4K, p =
253 0.271) but significantly downregulated p-eIF2α (Figure 4K). The ratio of p-eIF2α to
254 eIF2α was lower in the axon but not in the soma or dendritic region. These results suggest
255 that axonal distribution of mitochondria regulate the level of overall eIF2α protein and
256 local p-eIF2α.
257
258 **Depletion of axonal mitochondria suppressed global translation**
259 Phosphorylation of eIF2α induces conformational changes in the eIF2 complex and
260 inhibits global translation[36]. To analyze the effects of *milton* knockdown on translation,
261 we performed polysome gradient centrifugation to examine the level of ribosome binding
262 to mRNA. Since p-eIF2α was downregulated, we hypothesized that *milton* knockdown
263 would enhance translation. However, unexpectedly, we found that *milton* knockdown
264 significantly reduced the level of mRNAs associated with polysomes (Figure 5A and B).
265 We also compared the level of translation between the brains of control and *milton*
266 knockdown flies by assessing the incorporation of puromycin (Figure 5C). Puromycin
267 incorporation was lower in the brains of *milton* knockdown flies than in those of control
268 flies, while it was not statistically significant (Figure 5C, indicated by a bracket). These
269 data suggest that the depletion of axonal mitochondria suppresses global translation.
270
271 **eIF2β upregulation reduces the level of p-eIF2α, impairs autophagy, and decreases**
272 **locomotor function**
273 We were motivated to ask if eIF2β upregulation mediates autophagic defects caused by
274 *milton* knockdown. If so, neuronal overexpression of *eIF2β* would also induce autophagy
275 impairment. Neuronal overexpression of *eIF2β* increased LC3-II, while the LC3-II/LC3-
276 I ratio was not significantly different (Figure 6A and B). Overexpression of *eIF2β*
277 significantly increased the p62 level in the Triton X-100-soluble fraction (Figure 6C, 4-
278 fold vs. control, $p < 0.005$ (1% Triton X-100)) but not in the SDS-soluble fraction (Figure
279 6C, 2-fold vs. control, $p = 0.062$ (2% SDS)), as observed in brains of *milton* knockdown
280 flies (Figure 2B). These data suggest that neuronal overexpression of *eIF2β* accumulates
281 autophagic substrates.
282 Since *milton* knockdown reduced the p-eIF2α level (Figure 4K), we asked whether an
283 increase in eIF2β affects p-eIF2α. Neuronal overexpression of *eIF2β* did not affect the
284 eIF2α level but significantly decreased the p-eIF2α level (Figure 6D, E).
285 Depletion of axonal mitochondria causes age-dependent decline in locomotor function[24].
286 We found that neuronal overexpression of *eIF2β* also caused locomotor dysfunction

287 (Figure 6F). Locomotor functions were significantly impaired in those flies at 20-day-old
288 and worsened further during aging (Figure 6F, compare 4-, 20-, and 30-day-old). We
289 asked if *eIF2β* overexpression causes neurodegeneration, as depletion of axonal
290 mitochondria in the photoreceptor neurons causes axon degeneration in an age-dependent
291 manner[24]. *eIF2β* overexpression in photoreceptor neurons tends to increase
292 neurodegeneration in aged flies, while it was not statistically significant ($p>0.05$, Figure
293 S2).
294 These data indicate that an increase of eIF2β in neurons phenocopies depletion of axonal
295 mitochondria, including suppression of autophagy and age-dependent locomotor
296 dysfunction, and suggest that increase of eIF2β mediates these phenotypes downstream
297 of loss of axonal mitochondria.
298
299 **Lowering *eIF2β* rescues autophagic impairment and locomotor dysfunction induced**
300 **by *milton* knockdown**
301 Finally, we investigated whether suppression of eIF2β rescues autophagy impairment and
302 locomotor dysfunction caused by neuronal knockdown of *milton*. Null mutants and flies
303 with RNAi-mediated knockdown of *eIF2β* in neurons did not survive. Flies lacking one
304 copy of the *eIF2β* gene survived without any gross abnormality, and the level of *eIF2β*
305 mRNA in these flies was about 80% of that in control flies (Figure 7A). *eIF2β*
306 heterozygosity did not affect the eIF2α and p-eIF2α levels (Figure S3A and B).
307 Neuronal knockdown of *milton* causes accumulation of autophagic substrate p62 in the
308 Triton X-100-soluble fraction (Figure 2B), and we tested if lowering eIF2β ameliorates
309 it. We found that *eIF2β* heterozygosity caused a mild increase in LC3-I levels and
310 decreases in LC3-II levels, resulting in a significantly lower LC3-II/LC3-I ratio in *milton*
311 knockdown flies (Figure 7B). *eIF2β* heterozygosity decreased the p62 level in the Triton
312 X-100-soluble fraction in the brains of *milton* knockdown flies (Figure 7C). The p62 level
313 in the SDS-soluble fraction, which is not sensitive to *milton* knockdown (Figure 2B), was
314 not affected (Figure 7C). These results suggest that suppression of *eIF2β* ameliorates the
315 impairment of autophagy caused by *milton* knockdown.
316 *eIF2β* heterozygosity also rescued locomotor dysfunction induced by *milton* knockdown.
317 *milton* knockdown flies with *eIF2β* heterozygosity exhibited better locomotor function
318 than *milton* knockdown alone (Figure 7D). The *milton* mRNA level was not increased in
319 these flies, indicating that the rescue effect in the *eIF2β* heterozygous background was
320 not mediated by an increase in the *milton* mRNA level (Figure S3C). These data suggest
321 that eIF2β upregulation mediates autophagy impairment and locomotor dysfunction
322 caused by the depletion of axonal mitochondria.

Discussion

Proteostasis perturbations trigger the formation of pathological aggregates and increase the risks of neurodegenerative diseases during aging. By using neuronal *milton* knockdown to deplete mitochondria from the axon, we provide evidence that loss of axonal mitochondria drives age-related proteostasis collapse via eIF2β (Figure 8). We observed declines in autophagy-mediated degradation of less-aggregated proteins and proteasome activity in *milton* knockdown flies (Figure 2). Accumulation of ubiquitinated proteins and changes in age-related pathways started prematurely in *milton* knockdown flies (Figure 1 and Table 2). *milton* knockdown increased eIF2β and lowered eIF2α phosphorylation (Figure 4). Overexpression of *eIF2β* phenocopied the effects of *milton* knockdown, including reduced autophagy and accelerated age-related locomotor defects (Figure 6). Furthermore, lowering *eIF2β* levels suppressed the impairment of autophagy and locomotor dysfunction induced by *milton* knockdown (Figure 7). eIF2β protein levels are reduced at the 21-day-old; however, since a reduction in the eIF2β ameliorated *milton* knockdown-induced locomotor defects in aged flies (Figure 7), the reduction in eIF2β observed in the 21-day-old is not likely to negatively contribute to *milton* knockdown-induced defects. Our results suggest that mitochondrial distribution and eIF2β are part of the mechanisms constituting proteostasis.

milton knockdown causes loss of mitochondria in the axon and accumulation of mitochondria in the soma. Thus, the detrimental effects may be mediated by the accumulation of mitochondria. However, degeneration induced by *milton* knockdown is prominent in the axon and not detected in the cell body[24]. Furthermore, abnormal protein accumulation was observed in the axon (Figure 1), and p-eIF2α/eIF2α was decreased in the neurites but not in the soma (Figure 4), suggesting that proteostasis defects studied in this work are caused by depletion of mitochondria rather than accumulation of mitochondria. Further analyses to dissect the effects of *milton* knockdown on proteostasis and translation in the cell body and axon by experiments with spatial resolution would be needed.

The depletion of axonal mitochondria and accumulation of abnormal proteins are both characteristics of aged brains[37,38]. Our results suggest that the loss of axonal mitochondria is an event upstream of proteostasis collapse during aging. Neuronal knockdown of *milton* had more impact on proteostasis in young neurons than the old neurons (Figure 1).

359 Proteome analyses also showed that age-related pathways, such as immune responses, are
360 enhanced in young flies with *milton* knockdown (Table 2). The reduction in axonal
361 transport of mitochondria may be one of the triggering events of age-related changes and
362 accelerates the onset of aging in the brain. Disruption of proteostasis is expected to
363 contribute neurodegeneration[38] , and it would be interesting to analyze the sequence of
364 protein accumulation and axonal degeneration in *milton* knockdown ([24,29] and Figure 1)
365 in detail with higher time resolution.
366
367 Our results revealed that eIF2β regulates autophagy and maintains proteostasis during
368 aging. eIF2β is a component of eIF2, which meditates translational regulation and ISR
369 initiation. When ISR is activated, phosphorylated eIF2α suppresses global translation and
370 induces translation of ATF4, which mediates transcription of autophagy-related genes[39,40].
371 Since ISR can positively regulate autophagy, we suspected that suppression of ISR
372 underlies a reduction in autophagic protein degradation. We found neuronal knockdown
373 of *milton* reduced phosphorylated eIF2α, suggesting that ISR is reduced (Figure 4).
374 However, we also found that global translation was reduced (Figure 5). It may be possible
375 that increased levels of eIF2β disrupt the eIF2 complex or alter its functions. The
376 stoichiometric mismatch caused by an imbalance of eIF2 components may inhibit ISR
377 induction. Supporting this model, we found that eIF2β upregulation reduced the levels of
378 p-eIF2α (Figure 6). It is also possible that eIF2β mediates autophagy defects via
379 mechanisms independent of ISR since eIF2β has functions independent of eIF2[41,42]. For
380 example, suppression of *eIF2β* has been reported to slow down cancer cell growth[41]. In
381 developing neurons, eIF2β can directly interact with the translational repressor Kra to
382 regulate midline axon guidance[42]. However, to our knowledge, the roles of eIF2β in aging
383 have not been reported. Our results revealed a novel function of eIF2β to maintain
384 proteostasis during aging.
385
386 How depletion of axonal mitochondria upregulates eIF2β is currently under investigation.
387 A major mitochondrial function is ATP production, and depletion of axonal mitochondria
388 downregulates ATP in axons[33]. However, we found that ATP deprivation did not always
389 suppress autophagy (Figure 3), suggesting it is unlikely to be involved in the mechanisms
390 that induce eIF2β upregulation. Mitochondria also serve as signaling hubs for translation
391 and protein degradation. Mitochondrial proteins are regulated by co-translational protein
392 quality control, and mitochondrial damage induces translational stalling of mitochondrial
393 outer membrane-associated *complex-I 30 kD subunit* (*C-I30*) mRNA[43]. Additionally, the
394 mitochondrial outer membrane ubiquitin ligase MITOL (also known as MARCHF5)

395 ubiquitinates and regulates not only mitochondrial proteins such as Mfn2[44] but also
396 microtubule-associated[45] and endoplasmic reticulum[46] proteins. These findings indicate
397 that mitochondria serve as local signaling centers for proteostasis maintenance, and eIF2β
398 levels may also be regulated by mechanisms related to mitochondria.
399
400 In conclusion, our results suggest that axonal mitochondria and eIF2β form an axis to
401 maintain constitutive autophagy. Suppression of *eIF2β* rescued autophagic defects and
402 neuronal dysfunction upon loss of axonal mitochondria. Since eIF2β is conserved across
403 many species, including *Drosophila* and humans, our results suggest that eIF2β may be a
404 possible therapeutic target for aging and diseases associated with mitochondrial
405 mislocalization.
406
407
408 **Materials and methods**
409
410 **Fly stocks and husbandry**
411 Flies were maintained in standard cornmeal medium (10% glucose, 0.7% agar, 9%
412 cornmeal, 4% yeast extract, 0.3% propionic acid, and 0.1% n-butyl p-hydroxybenzoate)
413 at 25°C under light–dark cycles of 12:12 h. The flies were transferred to fresh food vials
414 for every 2–3 days. UAS-*milton* RNAi (v41508) was from VDRC and outcrossed to
415 [w1118] for five generations in our laboratory. Transgenic fly lines carrying UAS-
416 *luciferase* RNAi control for *milton* RNAi) was reported previously[24]. GMR-gal4, Elav-
417 gal4, UAS-*Pfk* RNAi (Bloomington stock center #36782), UAS-*luciferase* RNAi
418 (Bloomington stock center #31603) (control for *Pfk* RNAi), UAS-*GFP* (used for control
419 for UAS-*eIF2β*) and UAS-*eIF2β* (eIF2β^{EY08063}, Bloomington stock center #17425) were
420 from the Bloomington stock center. *eIF2β* heterozygous strain (PBac{SAstopDsRed}
421 LL07719, DGRC#142114) was from KYOTO *Drosophila* Stock Center. UAS-*mitoGFP*
422 was a kind gift from Drs. W. M. Saxton (University of California, Santa Cruz).
423
424 **Immunohistochemistry and image acquisition**
425 Fly brains were dissected in PBS and fixed for 45 minutes in formaldehyde (4% v/v in
426 PBS) at room temperature. After incubation in PBST containing 0.1% Triton X-100 for
427 10 min three times, samples were incubated for 1h at room temperature in PBST
428 containing 1% normal goat serum (Wako, #143-06561) and then incubated overnight with

429 the primary antibody (anti-ubiquitin antibody Ubi-1 (Thermo Fisher #13-1600) (1:50),
430 anti-eIF2α (abcam #ab26197) (1:50) and anti-p-eIF2α (Cell signaling #3398S) (1:50))
431 diluted in 1% NGS/PBST at 4 °C. Samples were then washed for 10 min with PBST
432 including 0.1% Triton X-100 three times and incubated with the secondary antibody for
433 overnight at 4° C. Brains were mounted in Vectashield (Vectorlab Cat#H-1100) and
434 analyzed under a confocal microscope (Nikon). Quantitative analysis was performed
435 using ImageJ (National Institutes of Health) with maximum projection images derived
436 from Z-stack images acquired with same settings. Puncta was identified with mean
437 intensity and area using ImageJ. For eIF2α and p- eIF2α immunostaining, the mushroom
438 body was detected by mitoGFP expression.
439
440 **Electron microscopy**
441 Proboscis was removed from decapitated heads, which were then incubated in primary
442 fixative solution (2.5% glutaraldehyde and 2% paraformaldehyde in 0.1 M sodium
443 cacodylate buffer) at R.T. for 2 hours. After washing heads with 3% sucrose in 0.1 M
444 sodium cacodylate buffer, fly heads were post-fixed for 1 hour in secondary fixation (1%
445 osmium tetroxide in 0.1 M sodium cacodylate buffer) on ice. After washing with H_2O,
446 heads were dehydrated with ethanol and infiltrated with propylene oxide and Epon
447 mixture (TAAB and Nissin EM) for 3 hours. After infiltration, specimens were embedded
448 with an Epon mixture at 70°C for 2~3 days. Thin sections (70 nm) of laminas were
449 collected on copper grids. The sections were stained with 5% uranyl acetate in 50%
450 ethanol and Reynolds' lead citrate solution. Electron micrographs were obtained with a
451 CCD Camera mounted on a JEM-1400 plus electron microscope (Jeol Ltd.). Quantitation
452 was performed using ImageJ (National Institutes of Health).
453
454 **SDS–PAGE and immunoblotting**
455 Western blotting was performed as reported previously[24]. Briefly, heads of 10-20
456 *Drosophila* were homogenized with SDS-Tris-Glycine sample buffer (0.312M Tris, 5%
457 SDS, 8% glycerol, 0.0625% BPB, 10% β-mercaptoethanol, 10μg/mL leupeptin, 0.4 μM
458 Pefabloc, 10mM β-glycerphosphate, 10mM NaF) and after boiling at 95ºC for 2 minutes,
459 it was centrifuged at 13,200 rpm, and the supernatant was used as a sample. For p62
460 western blot, fly heads were homogenized with 1% PBST and after centrifugation at
461 13,200 rpm, the supernatant was mixed 1:1 SDS-Tris-Glycine sample buffer, and boiled
462 at 95 ºC for 2 minutes. The pellet was dissolved with 2% SDS in PBS, then centrifuged
463 again at 13,200 rpm. The supernatant was mixed 1:1 SDS-Tris-Glycine sample buffer and
464 then boiled at 95 ºC for 2 minutes. SDS–PAGE for western blotting was performed using

465 15%(w/v) (LC3), 7.5%(w/v) (p62), 10% (w/v) (eIF2α, β, and p-eIF2α) polyacrylamide
466 gels. After electrophoresis, they were transferred to PVDF membrane (Merck Millipore)
467 using a transfer device (BIO-RAD). After transfer, the membrane was blocked with 5%
468 skim milk/TBST (50 mM Tris (pH 7.5), 0.15 M NaCl, 0.05% Tween20) for 1 hour and
469 incubated with primary antibody listed below overnight at 4 ºC. Membranes were rinsed
470 twice with TBST containing 0.65M NaCl and once with TBST containing 0.15M NaCl.
471 After incubation with the secondary antibody at room temperature for 1 hour, membranes
472 were rinsed twice with TBST containing 0.65M NaCl and once with TBST containing
473 0.15M NaCl. After incubation with Immobilon Western Chemiluminescent HRP
474 Substrate (Merck Millipore), chemiluminescent signals were detected with Fusion FX
475 (Vilber). Experiments were repeated at least 3 times with independent cohorts of flies.
476 Primary antibodies: anti-LC3 antibody Atg8 (Merck Millipore #ABC975) (1:1000), anti-
477 p62 antibody Ref2P (abcam #ab178440) (1:750), anti-eIF2β antibody (1:1500), anti-
478 eIF2α antibody (abcam #ab26197) (1:1000), anti-p-eIF2α antibody (Cell signaling
479 #3398S) (1:2000), anti-actin antibody (SIGMA A2066) (1:3000) and anti-β tubulin
480 antibody (Sigma #T9026) (1:800,000). Polyclonal anti-eIF2β antibody was raised against
481 a synthetic peptide (CGLEDDTKKEDPQDEA) corresponding to the C-terminal residues
482 29-43 of *Drosophila* eIF2β (1:1500).
483 Secondary antibodies: Peroxidase-conjugated goat anti-mouse IgG antibody (Dako
484 #P0447) (1:2000), peroxidase-conjugated pig anti-rabbit IgG antibody (Dako #P0399)
485 (1:2000)
486
487 **Proteasome assay**
488 Heads from ten flies were homogenized in 150 µl of buffer B (25 mM Tris-HCl [pH 7.5],
489 2 mM ATP, 5 mM MgCl2, and 1 mM dithiothreitol). Proteasome peptidase activity in the
490 lysates was measured with a synthetic peptide substrate, succinyl-Leu-Leu-Val-Tyr-7-
491 amino-4-methyl-coumarin (Suc-LLVY-AMC) (Cayman). Luminescence was measured
492 on a multimode plate reader 2300 Enspire (PerkinElmer). Experiments were repeated at
493 least 3 times with independent cohorts of flies.
494
495 **ATP assay**
496 Heads from the 10 flies were homogenized in 50 µl of 6 M guanidine-HCl in extraction
497 buffer (100 mM Tris and 4 mM EDTA, pH 7.8) to inhibit ATPases. Samples were boiled
498 for 5 min and centrifuged. The supernatant was diluted 4% with extraction buffer and
499 mixed with a reaction solution (ATP Determination kit, Invitrogen). Luminescence was
500 measured on a multimode plate reader 2300 Enspire (PerkinElmer). The relative ATP

501 levels were calculated by dividing the luminescence by the total protein concentration,
502 which was determined by the Bradford method. Experiments were repeated at least 3
503 times with independent cohorts of flies.
504
505 **Proteomic assay and pathway analysis**
506 *Sample preparation*
507 Heads from the 35 flies were homogenized in 110 µl of extraction buffer (0.25% RapiGest
508 SF, 50mM ammonium bicarbonate, 10mM dithiothreitol, 10µg/mL leupeptin, 0.4 µM
509 Pefabloc, 10mM β-glycerphosphate, 10mM NaF). Homogenized samples were
510 centrifuged and boiled for 5 min. After quantification of the protein concentration using
511 a Pierce® 660 nm Protein Assay (Thermo Fisher Scientific), 10 µg proteins from each
512 sample were reduced using 5 mM tris (2-carboxyethyl) phosphine hydrochloride (TCEP-
513 HCl; Thermo Fisher Scientific) at 60°C for 1 h, alkylated using 15 mM iodoacetamide
514 (Fujifilm Wako Pure Chemical, Osaka, Japan) at room temperature for 30 min, and then
515 digested using 1.5 µg Trypsin Gold (Mass Spectrometry Grade; Promega, Madison, WI,
516 USA) at 37°C for 17 h. The digests were acidified by the addition of trifluoroacetic acid
517 (TFA), incubated at 37°C for 30 min, and then centrifuged at 17,000 ×*g* for 10 min to
518 remove the RapiGest SF. The supernatants were collected and desalted using
519 MonoSpin™ C18 (GL Sciences, Tokyo, Japan). The resulting eluates were concentrated
520 *in vacuo*, dissolved in 2% MeCN containing 0.1% formic acid (FA), and subjected to LC-
521 MS/MS analysis.
522
523 *LC-MS/MS analysis and database search*
524 LC-MS/MS analyses were performed on an Ultimate 3000 RSLCnano system (Thermo
525 Fisher Scientific) coupled to a Q Exactive hybrid quadrupole-Orbitrap mass spectrometer
526 (Thermo Fisher Scientific) equipped with a nano electron spray ionization (ESI) source.
527 The LC system was equipped with a trap column (C18 PepMap 100, 0.3 × 5 mm, 5 µm,
528 Thermo Fisher Scientific) and an analytical column (NTCC-360/75-3-125, Nikkyo
529 Technos, Tokyo, Japan). Peptide separation was performed using a 90-min gradient of
530 water/0.1% FA (mobile phase A) and MeCN/0.1% FA (mobile phase B) at a flow rate of
531 300 nL/min. Elution was performed as follows: 0–3 min, 2% B; 3–93 min, 2%–40% B;
532 93–95 min, 40%–95% B; 95–105 min, 95% B; 105–107 min, 95%–2% B; and 107–120
533 min, 2% B. The mass spectrometer was operated in data-dependent acquisition mode. The
534 MS parameters were as follows: spray voltage, 2.0 kV; capillary temperature, 275°C; S-
535 lens RF level, 50; scan type, full MS; scan range, *m/z* 350–1500; resolution, 70,000;
536 polarity, positive; automatic gain control target, 3×10^6; and maximum injection time,

537 100 msec. The MS/MS parameters were as follows: resolution, 17,500; automatic gain
538 control target, 1×10^5; maximum injection time, 60 msec; normalized collision energy
539 (NCE), 27; dynamic exclusion, 15 sec; loop count, 10; isolation window, 1.6 *m/z*; charge
540 exclusion: unassigned, 1 and ≥8; and injection volume, 1 µL (containing 0.5 µg protein).
541 Measurements were made in duplicate for each sample.
542
543 The identification of proteins and label-free quantification (LFQ) of the detected peptides
544 were performed using Proteome Discoverer software ver. 2.4 (Thermo Fisher Scientific).
545 The analytical parameters used for the database search were as follows: parent mass error
546 tolerance, 10.0 ppm; fragment mass error tolerance, 0.02 Da; search engine, sequest HT;
547 protein database, Drosophila melanogaster (Fruit fly: SwissProt Tax ID=7227); enzyme
548 name, trypsin (full); maximum number of missed cleavages, 2; dynamic modification,
549 oxidation (methionine), phosphorylation (serine, threonine, tyrosine), acetyl (lysine), GG
550 (lysine); N-terminal modification, Met-loss (methionine), and Met-loss+acetyl
551 (methionine); static modification, carbamidomethylation (cysteine) and FDR confidence,
552 High < 0.01, 0.01 ≤ Medium < 0.05, 0.05 ≤ Low. The parameters for LFQ were as follows:
553 precursor abundance, based on area; and normalization mode, total peptide amount.
554 The abundance ratio of *milton* RNAi to control RNAi at 7 or 21 day-old was calculated.
555 We considered proteins with an abundance ratio of ≥2.0 or ≤ 0.5 and an ANOVA *P*-value
556 of < 0.05 based on volcano plots to be differentially expressed of *milton* RNAi. To extract
557 molecular networks biologically relevant to the proteins that are differentially expressed
558 in *milton* RNAi, pathway analysis was performed using KeyMolnet (KM Data Inc., Tokyo,
559 Japan).
560
561 **RNA extraction and quantitative real-time PCR analysis**
562 Heads from more than 25 flies were mechanically isolated, and total RNA was extracted
563 using ISOGEN (NipponGene) followed by reverse-transcription using PrimeScript RT
564 reagent kit (Takara). The resulting cDNA was used as a template for PCR with
565 THUNDERBIRD SYBR qPCR mix (TOYOBO) on a Thermal Cycler Dice real-time
566 system TP800 (Takara). Expression of genes of interest was standardized relative to rp49.
567 Relative expression values were determined by the ΔΔCT method (Livak and Schmittgen,
568 2001). Experiments were repeated three times, and a representative result was shown.
569 Primers were designed using DRSC FlyPrimerBank (Harvard Medical School). Primer
570 sequences are shown below;
571 *eIF2β* for 5′-GGACGACGACAAGAGCGAAG -3′
572 *eIF2β* rev 5′-CGGTCGCATCACGAACTTTG -3′

573 *milton* for 5′-GGCTTCAGGGCCAGGTATCT-3′
574 *milton* rev 5′-GCCGAACTTGGCTGACTTTG-3′
575 *Actin* for 5′-TGCACCGCAAGTGCTTCTAA-3′
576 *Actin* rev 5′-TGCTGCACTCCAAACTTCCA-3′
577 *rp49* for 5′-GCTAAGCTGTCGCACAAATG-3′
578 *rp49* rev 5′- GTTCGATCCGTAACCGATGT-3′
579
580 **Polysome gradient centrifugation**
581 30 heads were homogenized in 150 µl of lysis buffer (25 mM Tris pH 7.5, 50 mM MgCl2,
582 250 mM NaCl, 1 mM DTT, 0.5 mg/ml cycloheximide, 0.1 mg/ml heparin). The lysates
583 were centrifuged at 13,200 rpm at 4 °C for 5 minutes, and the supernatant was collected.
584 The samples containing 38µg of RNA was layered gently on top of a 10–50% w/w sucrose
585 gradient (50 mM Tris pH 7.5, 50 mM MgCl2, 250 mM NaCl, 0.1 mg/ml heparin, 0.5
586 mg/ml cycloheximide in 5 ml polyallomer tube) and centrifuged at 37,000 rpm at 4°C for
587 150 minutes in a himac CP-NX ultracentrifuge using a P50AT rotor. Samples were
588 fractionated from top to bottom, and absorbance at OD260 nm was analyzed by a Plate
589 reader (EnSpire). Experiments were repeated at least 3 times with independent cohorts of
590 flies.
591
592 **Puromycin analysis**
593 13-day-old flies were starved for 6 hr and fed 600 µM puromycin (Sigma) or 600 µM
594 puromycin/35 mM cycloheximide (Sigma) in 5% sucrose solution for 20 hr. Incorporated
595 puromycin was quantified by western blot with anti-puromycin antibody and normalized
596 with actin. Experiments were repeated at least 3 times with independent cohorts of flies.
597
598 **Histological analysis**
599 Fly heads were fixed in Bouin's fixative solution for 48 h at room temperature, incubated
600 for 24 h in 50 mM Tris/150 mM NaCl, and embedded in paraffin. Serial sections (7 µm
601 thickness) through the entire heads were stained with hematoxylin and eosin and
602 examined by bright-field microscopy. Images of the sections that include the lamina were
603 captured with Keyence microscope BZ-X700 (Keyence), and the vacuole area was
604 measured using ImageJ (National Institutes of Health).
605
606 **Climbing assay**
607 The climbing assay was performed as previously described[24]. Flies were placed in an
608 empty plastic vial (2.5 cm in diameter × 10 cm in length). The vial was gently tapped to

knock the flies to the bottom, and the number of flies reached to the top, middle and bottom areas of the vials in 10 s was counted. Experiments were repeated 10 times, and the mean percentage of flies in each area and standard deviations were calculated. Experiments were repeated with independent cohorts more than three times, and a representative result was shown.

Statistics

The number of replicates, what n represents, precision measurements, and the meaning of error bars are indicated in Figure Legends. Data are shown as means ± SEM. For pairwise comparisons, Student's t-test was performed with Microsoft Excel (Microsoft). For multiple comparisons, data were analyzed using one-way ANOVA with Tukey's HSD multiple-comparisons test in the GraphPad Prism 6.0 software (GraphPad Software, Inc., La Jolla, CA). Results with a p-value of less than 0.05 were considered to be statistically significant.

Acknowledgments

The authors thank the Bloomington stock center; TRiP at Harvard Medical School (NIH/NIGMS R01-GM084947); the Kyoto Drosophila Stock Center and the Vienna Drosophila RNAi Center for fly stocks. The authors thank Dr. Masayuki Miura from Department of Pharmaceutical Science, University of Tokyo, for proteasome activity assay protocol; Dr. Shin-ichi Hisanaga from the Department of Biological Sciences, Tokyo Metropolitan University, for critical comments; Dr. Taro Saito, Dr. Akiko Asada from the Department of Biological Sciences, Tokyo Metropolitan University, Dr. Michiko Sekiya from Department of Alzheimer's Disease Research, National Center for Geriatrics and Gerontology, and Dr. Seiji Watanabe, Dr. Koji Yamanaka from Department of Neuroscience and Pathobiology, Research Institute of Environmental Medicine, Nagoya University for technical supports.

Funding

This work was supported by the Sasakawa Scientific Research Grant (2021-4087) (to K.S.), the Takeda Science Foundation (to KA), Hoansha foundation grant (to KA), a research award from the Japan Foundation for Aging and Health (to KA), the Novartis Foundation (Japan) for the promotion of Science (to KA), a Grant-in-Aid for Scientific Research on Challenging Research (Exploratory) [JSPS KAKENHI Grant number

19K21593] (to KA), NIG-JOINT (National Institute of Genetics, 71A2018, 25A2019) (to K.A.) and TMU strategic research fund for social engagement (to KA).

Author contributions

K.S. and K.A. designed the experiments, interpreted the data, and wrote the manuscript; K.S., Y.M., K.M.I and E.S. conducted the experiments, and K.S., Y.M., E.S., and K.A. analyzed the data. All authors read and approved the manuscript.

Declaration of interests

The authors declare no competing interests.

Data Availability

The datasets used and/or analyzed during the current study are available from the corresponding author upon request.

Figure legends

Figure 1. Knockdown of *milton* or *Miro* causes protein accumulation in the axon

(A) Schematic representation of the mitochondrial transport machinery. Knockdown of *milton*, an adapter protein for mitochondrial transport, depletes mitochondria in the axon. (B, C) Ubiquitinated proteins in brains with neuronal knockdown of *milton* or *Miro*. Brains dissected at 14-day-old (B) or 30-day-old (C) were immunostained with an antibody against ubiquitin. Firefly *luciferase* RNAi was used as a control. Representative images (left) and quantitation of the number of ubiquitin-positive puncta (right) are shown. Scale bars of hemibrains, 100 µm, Scale bars of high magnifications, 10 µm. Means ± SE, n = 8. *N.S.*, $p > 0.05$; ***$p < 0.005$ (one-way analysis of variance (ANOVA) followed by Tukey's honestly significant difference (HSD) *post hoc* test). (D) Cross sections in the lamina and in the retina were used to analyze the ultrastructure of synapses and cell bodies, respectively. *milton* RNAi was expressed in the retina and neurons via a combination of GAL4 drivers, a pan-retinal gmr-GAL4 and pan-neuronal elav-GAL4. (E) Quantitation of the number of mitochondria in a presynaptic terminal from transmission electron micrographs. 180 presynaptic terminals from cross-sections of the lamina from three

681 brains were analyzed. ***$p < 0.005$ (Chi-square test). (F, G) Presynaptic terminals of
682 photoreceptor neurons of control and *milton* knockdown flies. Photoreceptor neurons are
683 highlighted in blue. Swollen presynaptic terminals (asterisks in (F)), characterized by the
684 enlargement and higher circularity, were found more frequently in *milton* knockdown
685 neurons. Arrowheads indicate presynaptic terminals with dense materials. Scale bars, 2
686 μm. Representative images (Left) and quantitation (Right) are shown. 918–1118 from
687 three heads were quantified for the percentage of swollen presynaptic terminals, and 180
688 presynaptic terminals from three heads were quantified for the size of presynaptic
689 terminals. Mean ± SE, **$p < 0.01$, ***$p < 0.005$ (Student's *t*-test). (G) Dense materials
690 (arrowheads in (G)) in the presynaptic terminals of *milton* knockdown neurons. Scale bars,
691 2 μm. The ratio of presynaptic terminals containing dense materials were quantified from
692 918–1118 presynaptic terminals from three heads. Mean ± SE, ***$p < 0.005$ (Student's *t*-
693 test). (H) Cell bodies of photoreceptor neurons of control and *milton* knockdown flies.
694 Scale bars, 2 μm. Flies were 27-day-old.
695
696 **Figure 2. *milton* knockdown impairs protein degradation pathways**
697 (A, B) Western blotting of head extracts of control and *milton* knockdown flies with
698 antibodies against LC3 (A) and Ref2P, the fly homolog of mammalian p62 (B). For the
699 analyses of p62 levels, heads were extracted with 1% Triton X-100 or 2% SDS (B). Flies
700 were 14-day-old. Representative blots (left) and quantitation (right) are shown. Actin was
701 used as a loading control. Means ± SE, n = 6 (LC3), n = 3 (p62). (C) Proteasome activity
702 in head extracts of control and *milton* knockdown flies was measured by hydrolysis of
703 Suc-LLVY-AMC at 14-day-old. Means ± SE, n = 3. (D, E) Western blotting of head
704 extracts of 30-day-old control and *milton* knockdown flies. Blotting was performed with
705 anti-LC3 (D) and anti-p62 (E) antibodies. Representative blots (left) and quantitation
706 (right) are shown. Actin was used as a loading control. Means ± SE, n = 6 (LC3), n = 3
707 (p62). (F) Proteasome activity in head extracts of 30-day-old control and *milton*
708 knockdown flies. Means ± SE, n = 3. *N.S.*, $p > 0.05$; *$p < 0.05$; **$p < 0.01$; ***$p < 0.005$
709 (Student's *t*-test).
710
711 **Figure 3. ATP deprivation does not impair autophagy**
712 (A-C) ATP levels in brain extracts of control and *milton* knockdown flies (A) and control
713 and *Pfk* knockdown flies (B) and comparison of the effects of *milton* knockdown and *Pfk*
714 knockdown on ATP levels (C). Flies were 14 day-old. Means ± SE, n = 3. (D, E) Western
715 blotting of head extracts of flies with neuronal expression of control or *Pfk* RNAi. Blotting
716 was performed with anti-LC3 (D) and anti-p62 (E) antibodies. For analyses of p62 levels,

717 heads were extracted with 1% Triton X-100 or 2% SDS. Representative blots (left) and
718 quantitation (right) are shown. Actin was used as a loading control. Means ± SE, n = 6
719 (LC3), n = 3 (p62). (F) Proteasome activity in head lysates of flies with neuronal
720 expression of control or *Pfk* RNAi was measured by hydrolysis of Suc-LLVY-AMC.
721 Means ± SE, n = 3. *N.S.*, $p > 0.05$; *$p < 0.05$; **$p < 0.01$; ***$p < 0.005$ (Student's *t*-test).
722 Flies were at 14 day-old.
723
724 **Figure 4. *milton* knockdown upregulates eIF2β and decreases phosphorylation of**
725 **eIF2α and translation**
726 (A) Timing of proteome analysis and phenotypes observed in *milton* knockdown flies. (B,
727 C) Scatter plots of the $\log_2$ abundance ratio (x-axis) against the $-\log_{10}$ p-value (y-axis) of
728 proteins at 7-day-old (B) and 21-day-old (C). (D) eIF2 subunit protein levels from
729 proteome analysis of *milton* knockdown flies compared to those of control flies. (E)
730 Western blotting of head extracts of flies expressing control or *milton* RNAi in neurons
731 with an anti-eIF2β antibody. Flies were 14-day-old. Representative blots (left) and
732 quantitation (right) are shown. Tubulin was used as a loading control. Means ± SE, n = 6.
733 (F) *eIF2β* mRNA levels quantified by qRT-PCR. Means ± SE, n = 4, (G, H) Western
734 blotting of head extracts with anti-eIF2α (G) and anti-p-eIF2α (H) antibodies. Flies were
735 14-day-old. Representative blots (left) and quantitation (right) are shown. Tubulin was
736 used as a loading control. Means ± SE, n = 6. (I) A schematic representation of the axon
737 (Lobe tips), the cell body region (Kenyon cells), and dendritic region (Calyxes) in the fly
738 brain. Scale bars, 100μm. (J, K) Immunostaining with anti-eIF2α and anti-p-eIF2α
739 antibodies. The mushroom body was identified by expression of mito-GFP. Scale bars,
740 20μm. The signal intensities of eIF2α and p-eIF2α in axons, dendrites, and cell bodies
741 were quantified and are shown as ratios relative to the control. Means ± SE, n=12.
742 *N.S.*, $p > 0.05$; *$p < 0.05$; **$p < 0.01$; ***$p < 0.005$ (Student's *t*-test).
743
744 **Figure 5. *milton* knockdown suppressed global translation**
745 (A) Representative polysome traces of head lysates of control and *milton* knockdown flies.
746 (B) Quantitation of polysome fraction. The relative ratio of area under the curve (AUC)
747 of polysome fractions (sedimentation 28%-50%). Means ± SE, n = 3. ***$p < 0.005$
748 (Student's *t*-test) (C) Western blotting of head lysates of control and *milton* knockdown
749 flies fed puromycin alone or puromycin and cycloheximide (CHX) with an anti-
750 puromycin antibody. Flies were 14-day-old. Actin was used as a loading control.
751 Representative blots (left) and quantitation (right) are shown. Means ± SE, n = 3.
752 Student's *t*-test.

753

754 **Figure 6. eIF2β upregulation impairs autophagy and decreases locomotor function**
755 (A) *eIF2β* mRNA levels in head extracts of flies with UAS-*eIF2β* driven by elav-Gal4
756 (*eIF2β* OE) or UAS-GFP driven by elav-Gal4 (control) were quantified by qRT-PCR.
757 Flies were 2-day-old. Means ± SE, n=4. (B, C) Western blotting of head extracts with
758 anti-LC3 (B) and anti-p62 (C) antibodies. Flies were 14-day-old. Representative blots
759 (left) and quantitation (right) are shown. Tubulin and actin were used as loading controls.
760 Means ± SE, n = 3 (p62), n = 5 (LC3). (D, E) Western blotting of head extracts with anti-
761 eIF2α (D) and anti-p-eIF2α (E) antibodies. Flies were 14-day-old. Representative blots
762 (left) and quantitation (right) are shown. Tubulin was used as a loading control. Means ±
763 SE, n = 6. (F) Climbing assay revealed early-onset of age-dependent locomotor defects
764 in *eIF2β*-overexpressing flies. Means ± SE, n = 5. *N.S.*, $p > 0.05$; ***$p < 0.005$
765 (Student's *t*-test).
766

767 **Figure 7. Lowering *eIF2β* rescues autophagic impairment and locomotor**
768 **dysfunction induced by *milton* knockdown**
769 (A) *eIF2β* mRNA levels with one disrupted copy of the *eIF2β* gene
770 (*eIF2β*SAstopDsRed/+ (*eIF2β* -/+)). Head extracts of flies 2–3 day-old were analyzed by
771 qRT-PCR. Means ± SE, n = 3. (B, C) Western blotting of head extracts of flies with
772 neuronal expression of *milton* RNAi with or without *eIF2β* heterozygosity with anti-LC3
773 (B) and anti-p62 (C) antibodies. Flies were 14-day-old. Representative blots (left) and
774 quantitation (right) are shown. Actin was used as a loading control. Means ± SE, n = 5
775 (LC3), n = 3 (p62). (D) The climbing ability of 20-day-old flies expressing *milton* RNAi
776 with or without *eIF2β* heterozygosity. Means ± SE, n = 15. *N.S.*, $p > 0.05$; *$p < 0.05$;
777 ***$p < 0.005$ (Student's *t*-test).
778

779 **Figure 8. Graphical abstract: the mitochondria-eIF2β axis in the axon maintains**
780 **neuronal proteostasis during aging**
781
782

783 **Supplemental Figure 1. Ubiquitinated proteins in brains with neuronal knockdown**
784 **of *milton* at 1-day-old**
785 Brains dissected at 1-day-old were immunostained with an antibody against ubiquitin.
786 Representative images (left) and quantitation of the number of ubiquitin-positive puncta
787 (right) are shown. Scale bars of hemibrains, 100 μm, Means ± SE, n = 8. *N.S.*, $p > 0.05$
788 (Student's *t*-test).

789

790 **Supplemental Figure 2**. **Histology analysis of fly heads with *eIF2β* overexpression**
791 The morphology of the eye with eIF2β overexpression. The dotted lines indicate the retina.
792 Vacuoles are indicated by arrows. Representative images (left) and quantification of
793 vacuole area (right). The flies were 40-day-old. Means ± SE, n = 5-13 *N.S.*, $p > 0.05$
794 (Student's *t*-test).
795

796 **Supplemental Figure 3**. **Lowering the eIF2β level does not affect the levels of eIF2α**
797 **and p-eIF2α.**
798 (A, B) Blotting was performed with anti-eIF2α (A) and anti-p-eIF2α (B) antibodies. Flies
799 were 14-day-old. Representative blots (left) and quantitation (right) are shown. Tubulin
800 was used as a loading control. Means ± SE, n = 6. (C) *eIF2β* gene disruption does not
801 affect the knockdown efficiency of *milton*. *milton* mRNA levels in head extracts were
802 quantified by qRT-PCR. Flies were 2-day-old. Means ± SE, n = 3. *N.S.*, $p > 0.05$; $*p <$
803 0.05 (Student's *t*-test).
804
805
806

807 **References**

808 1. Yerbury, J.J., Ooi, L., Dillin, A., Saunders, D.N., Hatters, D.M., Beart, P.M., Cashman,
809 N.R., Wilson, M.R., and Ecroyd, H. (2016). Walking the tightrope: proteostasis and
810 neurodegenerative disease. J. Neurochem. *137*, 489-505. 10.1111/jnc.13575.
811 2. Hetz, C. (2021). Adapting the proteostasis capacity to sustain brain healthspan. Cell *184*,
812 1545-1560. 10.1016/j.cell.2021.02.007.
813 3. Balch, W.E., Morimoto, R.I., Dillin, A., and Kelly, J.W. (2008). Adapting proteostasis for
814 disease intervention. Science *319*, 916-919. 10.1126/science.1141448.
815 4. Kimball, S.R. (1999). Eukaryotic initiation factor eIF2. Int J Biochem Cell Biol *31*, 25-29.
816 10.1016/s1357-2725(98)00128-9.
817 5. Jackson, R.J., Hellen, C.U., and Pestova, T.V. (2010). The mechanism of eukaryotic
818 translation initiation and principles of its regulation. Nat. Rev. Mol. Cell Biol. *11*, 113-127.
819 10.1038/nrm2838.
820 6. Pakos-Zebrucka, K., Koryga, I., Mnich, K., Ljujic, M., Samali, A., and Gorman, A.M.
821 (2016). The integrated stress response. EMBO Rep *17*, 1374-1395.
822 10.15252/embr.201642195.
823 7. Kroemer, G., Marino, G., and Levine, B. (2010). Autophagy and the integrated stress
824 response. Mol. Cell *40*, 280-293. 10.1016/j.molcel.2010.09.023.

825 8. Nandi, D., Tahiliani, P., Kumar, A., and Chandu, D. (2006). The ubiquitin-proteasome
826 system. J Biosci *31*, 137-155. 10.1007/BF02705243.
827 9. Glick, D., Barth, S., and Macleod, K.F. (2010). Autophagy: cellular and molecular
828 mechanisms. J. Pathol. *221*, 3-12. 10.1002/path.2697.
829 10. Vargas, J.N.S., Hamasaki, M., Kawabata, T., Youle, R.J., and Yoshimori, T. (2023). The
830 mechanisms and roles of selective autophagy in mammals. Nat. Rev. Mol. Cell Biol. *24*,
831 167-185. 10.1038/s41580-022-00542-2.
832 11. Aman, Y., Schmauck-Medina, T., Hansen, M., Morimoto, R.I., Simon, A.K., Bjedov, I.,
833 Palikaras, K., Simonsen, A., Johansen, T., Tavernarakis, N., et al. (2021). Autophagy in
834 healthy aging and disease. Nat Aging *1*, 634-650. 10.1038/s43587-021-00098-4.
835 12. Ross, C.A., and Poirier, M.A. (2004). Protein aggregation and neurodegenerative disease.
836 Nat. Med. *10 Suppl*, S10-17. 10.1038/nm1066.
837 13. Rubinsztein, D.C., Marino, G., and Kroemer, G. (2011). Autophagy and aging. Cell *146*,
838 682-695. 10.1016/j.cell.2011.07.030.
839 14. Vos, M., Lauwers, E., and Verstreken, P. (2010). Synaptic mitochondria in synaptic
840 transmission and organization of vesicle pools in health and disease. Front Synaptic
841 Neurosci *2*, 139. 10.3389/fnsyn.2010.00139.
842 15. Cheng, A., Hou, Y., and Mattson, M.P. (2010). Mitochondria and neuroplasticity. ASN
843 Neuro *2*, e00045. 10.1042/AN20100019.
844 16. Hollenbeck, P.J., and Saxton, W.M. (2005). The axonal transport of mitochondria. J. Cell
845 Sci. *118*, 5411-5419. 10.1242/jcs.02745.
846 17. Takihara, Y., Inatani, M., Eto, K., Inoue, T., Kreymerman, A., Miyake, S., Ueno, S.,
847 Nagaya, M., Nakanishi, A., Iwao, K., et al. (2015). In vivo imaging of axonal transport of
848 mitochondria in the diseased and aged mammalian CNS. Proc Natl Acad Sci U S A *112*,
849 10515-10520. 10.1073/pnas.1509879112.
850 18. Milde, S., Adalbert, R., Elaman, M.H., and Coleman, M.P. (2015). Axonal transport
851 declines with age in two distinct phases separated by a period of relative stability.
852 Neurobiol. Aging *36*, 971-981. 10.1016/j.neurobiolaging.2014.09.018.
853 19. Vagnoni, A., Hoffmann, P.C., and Bullock, S.L. (2016). Reducing Lissencephaly-1 levels
854 augments mitochondrial transport and has a protective effect in adult Drosophila neurons.
855 J. Cell Sci. *129*, 178-190. 10.1242/jcs.179184.
856 20. Morsci, N.S., Hall, D.H., Driscoll, M., and Sheng, Z.H. (2016). Age-Related Phasic
857 Patterns of Mitochondrial Maintenance in Adult Caenorhabditis elegans Neurons. J.
858 Neurosci. *36*, 1373-1385. 10.1523/JNEUROSCI.2799-15.2016.
859 21. Adalbert, R., and Coleman, M.P. (2013). Review: Axon pathology in age-related
860 neurodegenerative disorders. Neuropathol. Appl. Neurobiol. *39*, 90-108. 10.1111/j.1365-

861 2990.2012.01308.x.
862 22. Duncan, J.E., and Goldstein, L.S. (2006). The genetics of axonal transport and axonal
863 transport disorders. PLoS Genet. *2*, e124. 10.1371/journal.pgen.0020124.
864 23. Chen, H., and Chan, D.C. (2009). Mitochondrial dynamics--fusion, fission, movement,
865 and mitophagy--in neurodegenerative diseases. Hum. Mol. Genet. *18*, R169-176.
866 10.1093/hmg/ddp326.
867 24. Iijima-Ando, K., Sekiya, M., Maruko-Otake, A., Ohtake, Y., Suzuki, E., Lu, B., and Iijima,
868 K.M. (2012). Loss of axonal mitochondria promotes tau-mediated neurodegeneration and
869 Alzheimer's disease-related tau phosphorylation via PAR-1. PLoS Genet. *8*, e1002918.
870 10.1371/journal.pgen.1002918.
871 25. Lopez-Domenech, G., Higgs, N.F., Vaccaro, V., Ros, H., Arancibia-Carcamo, I.L.,
872 MacAskill, A.F., and Kittler, J.T. (2016). Loss of Dendritic Complexity Precedes
873 Neurodegeneration in a Mouse Model with Disrupted Mitochondrial Distribution in
874 Mature Dendrites. Cell Rep *17*, 317-327. 10.1016/j.celrep.2016.09.004.
875 26. Guo, X., Macleod, G.T., Wellington, A., Hu, F., Panchumarthi, S., Schoenfield, M., Marin,
876 L., Charlton, M.P., Atwood, H.L., and Zinsmaier, K.E. (2005). The GTPase dMiro is
877 required for axonal transport of mitochondria to Drosophila synapses. Neuron *47*, 379-
878 393. 10.1016/j.neuron.2005.06.027.
879 27. Glater, E.E., Megeath, L.J., Stowers, R.S., and Schwarz, T.L. (2006). Axonal transport of
880 mitochondria requires milton to recruit kinesin heavy chain and is light chain independent.
881 J. Cell Biol. *173*, 545-557. 10.1083/jcb.200601067.
882 28. Stowers, R.S., Megeath, L.J., Gorska-Andrzejak, J., Meinertzhagen, I.A., and Schwarz, T.L.
883 (2002). Axonal transport of mitochondria to synapses depends on milton, a novel
884 Drosophila protein. Neuron *36*, 1063-1077. 10.1016/s0896-6273(02)01094-2.
885 29. Iijima-Ando, K., Hearn, S.A., Shenton, C., Gatt, A., Zhao, L., and Iijima, K. (2009).
886 Mitochondrial mislocalization underlies Abeta42-induced neuronal dysfunction in a
887 Drosophila model of Alzheimer's disease. PLoS One *4*, e8310.
888 10.1371/journal.pone.0008310.
889 30. Tonoki, A., Kuranaga, E., Tomioka, T., Hamazaki, J., Murata, S., Tanaka, K., and Miura,
890 M. (2009). Genetic evidence linking age-dependent attenuation of the 26S proteasome
891 with the aging process. Mol. Cell. Biol. *29*, 1095-1106. 10.1128/MCB.01227-08.
892 31. Klionsky, D.J., Abdel-Aziz, A.K., Abdelfatah, S., Abdellatif, M., Abdoli, A., Abel, S.,
893 Abeliovich, H., Abildgaard, M.H., Abudu, Y.P., Acevedo-Arozena, A., et al. (2021).
894 Guidelines for the use and interpretation of assays for monitoring autophagy (4th
895 edition)(1). Autophagy *17*, 1-382. 10.1080/15548627.2020.1797280.
896 32. Bartlett, B.J., Isakson, P., Lewerenz, J., Sanchez, H., Kotzebue, R.W., Cumming, R.C.,

897 Harris, G.L., Nezis, I.P., Schubert, D.R., Simonsen, A., and Finley, K.D. (2011). p62,
898 Ref(2)P and ubiquitinated proteins are conserved markers of neuronal aging, aggregate
899 formation and progressive autophagic defects. Autophagy *7*, 572-583.
900 10.4161/auto.7.6.14943.
901 33. Oka, M., Suzuki, E., Asada, A., Saito, T., Iijima, K.M., and Ando, K. (2021). Increasing
902 neuronal glucose uptake attenuates brain aging and promotes life span under dietary
903 restriction in Drosophila. iScience *24*, 101979. 10.1016/j.isci.2020.101979.
904 34. Zia, A., Pourbagher-Shahri, A.M., Farkhondeh, T., and Samarghandian, S. (2021).
905 Molecular and cellular pathways contributing to brain aging. Behav Brain Funct *17*, 6.
906 10.1186/s12993-021-00179-9.
907 35. Haigis, M.C., and Yankner, B.A. (2010). The aging stress response. Mol. Cell *40*, 333-344.
908 10.1016/j.molcel.2010.10.002.
909 36. Wek, R.C. (2018). Role of eIF2alpha Kinases in Translational Control and Adaptation to
910 Cellular Stress. Cold Spring Harb Perspect Biol *10*. 10.1101/cshperspect.a032870.
911 37. Currais, A., Fischer, W., Maher, P., and Schubert, D. (2017). Intraneuronal protein
912 aggregation as a trigger for inflammation and neurodegeneration in the aging brain.
913 FASEB J. *31*, 5-10. 10.1096/fj.201601184.
914 38. Grimm, A., and Eckert, A. (2017). Brain aging and neurodegeneration: from a
915 mitochondrial point of view. J. Neurochem. *143*, 418-431. 10.1111/jnc.14037.
916 39. Bond, S., Lopez-Lloreda, C., Gannon, P.J., Akay-Espinoza, C., and Jordan-Sciutto, K.L.
917 (2020). The Integrated Stress Response and Phosphorylated Eukaryotic Initiation Factor
918 2alpha in Neurodegeneration. J. Neuropathol. Exp. Neurol. *79*, 123-143.
919 10.1093/jnen/nlz129.
920 40. B'Chir, W., Maurin, A.C., Carraro, V., Averous, J., Jousse, C., Muranishi, Y., Parry, L.,
921 Stepien, G., Fafournoux, P., and Bruhat, A. (2013). The eIF2alpha/ATF4 pathway is
922 essential for stress-induced autophagy gene expression. Nucleic Acids Res. *41*, 7683-7699.
923 10.1093/nar/gkt563.
924 41. Salton, G.D., Laurino, C., Mega, N.O., Delgado-Canedo, A., Setterblad, N., Carmagnat,
925 M., Xavier, R.M., Cirne-Lima, E., Lenz, G., Henriques, J.A.P., and Laurino, J.P. (2017).
926 Deletion of eIF2beta lysine stretches creates a dominant negative that affects the
927 translation and proliferation in human cell line: A tool for arresting the cell growth. Cancer
928 Biol Ther *18*, 560-570. 10.1080/15384047.2017.1345383.
929 42. Lee, S., Nahm, M., Lee, M., Kwon, M., Kim, E., Zadeh, A.D., Cao, H., Kim, H.J., Lee,
930 Z.H., Oh, S.B., et al. (2007). The F-actin-microtubule crosslinker Shot is a platform for
931 Krasavietz-mediated translational regulation of midline axon repulsion. Development *134*,
932 1767-1777. 10.1242/dev.02842.

933 43. Wu, Z., Tantray, I., Lim, J., Chen, S., Li, Y., Davis, Z., Sitron, C., Dong, J., Gispert, S.,
934 Auburger, G., et al. (2019). MISTERMINATE Mechanistically Links Mitochondrial
935 Dysfunction with Proteostasis Failure. Mol. Cell *75*, 835-848 e838.
936 10.1016/j.molcel.2019.06.031.
937 44. Sugiura, A., Nagashima, S., Tokuyama, T., Amo, T., Matsuki, Y., Ishido, S., Kudo, Y.,
938 McBride, H.M., Fukuda, T., Matsushita, N., et al. (2013). MITOL regulates endoplasmic
939 reticulum-mitochondria contacts via Mitofusin2. Mol. Cell *51*, 20-34.
940 10.1016/j.molcel.2013.04.023.
941 45. Yonashiro, R., Kimijima, Y., Shimura, T., Kawaguchi, K., Fukuda, T., Inatome, R., and
942 Yanagi, S. (2012). Mitochondrial ubiquitin ligase MITOL blocks S-nitrosylated MAP1B-
943 light chain 1-mediated mitochondrial dysfunction and neuronal cell death. Proc Natl Acad
944 Sci U S A *109*, 2382-2387. 10.1073/pnas.1114985109.
945 46. Takeda, K., Nagashima, S., Shiiba, I., Uda, A., Tokuyama, T., Ito, N., Fukuda, T.,
946 Matsushita, N., Ishido, S., Iwawaki, T., et al. (2019). MITOL prevents ER stress-induced
947 apoptosis by IRE1alpha ubiquitylation at ER-mitochondria contact sites. EMBO J. *38*,
948 e100999. 10.15252/embj.2018100999.
949

Shinno et. al., Figure 1

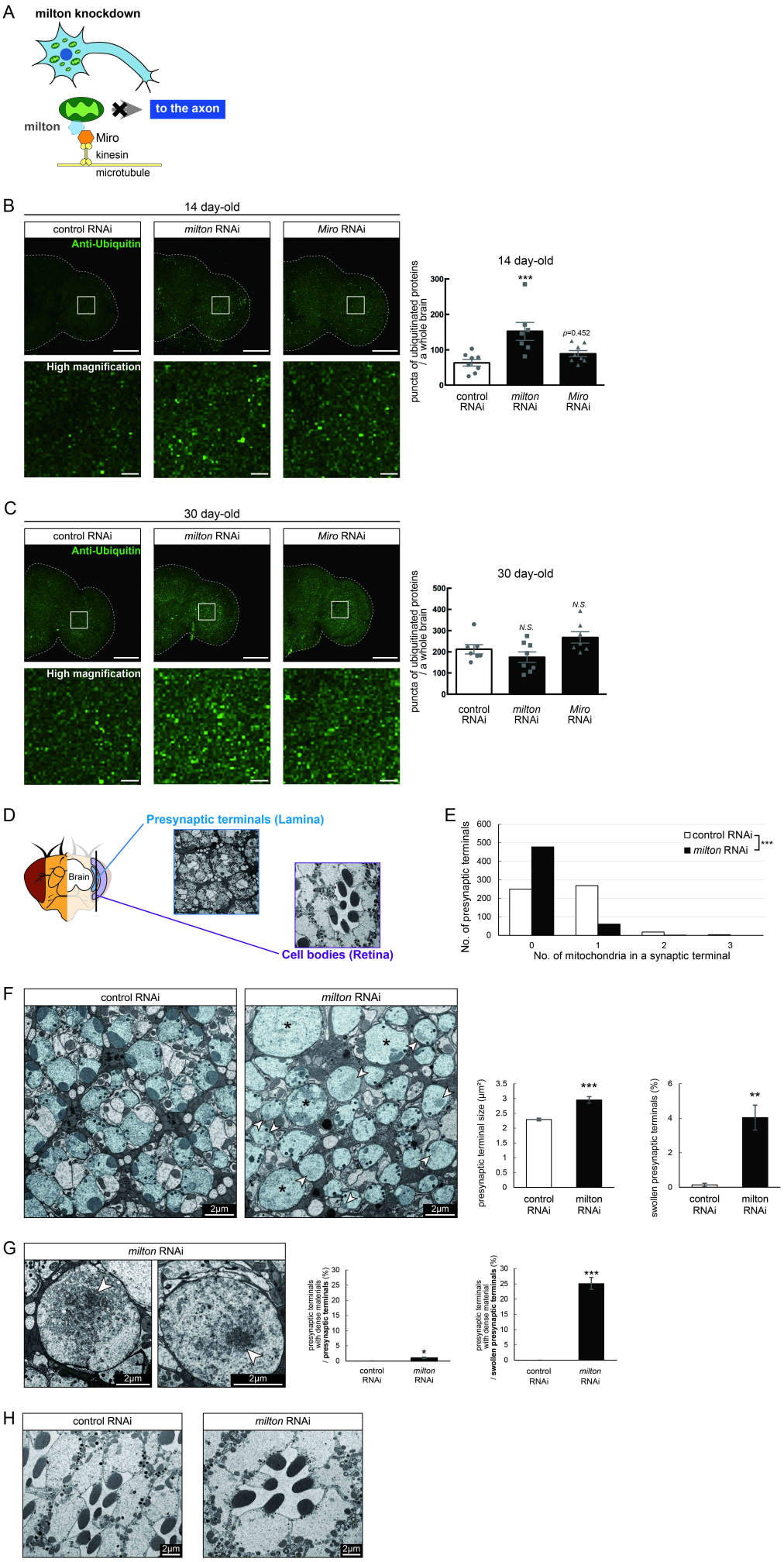

Shinno et. al., Figure 2

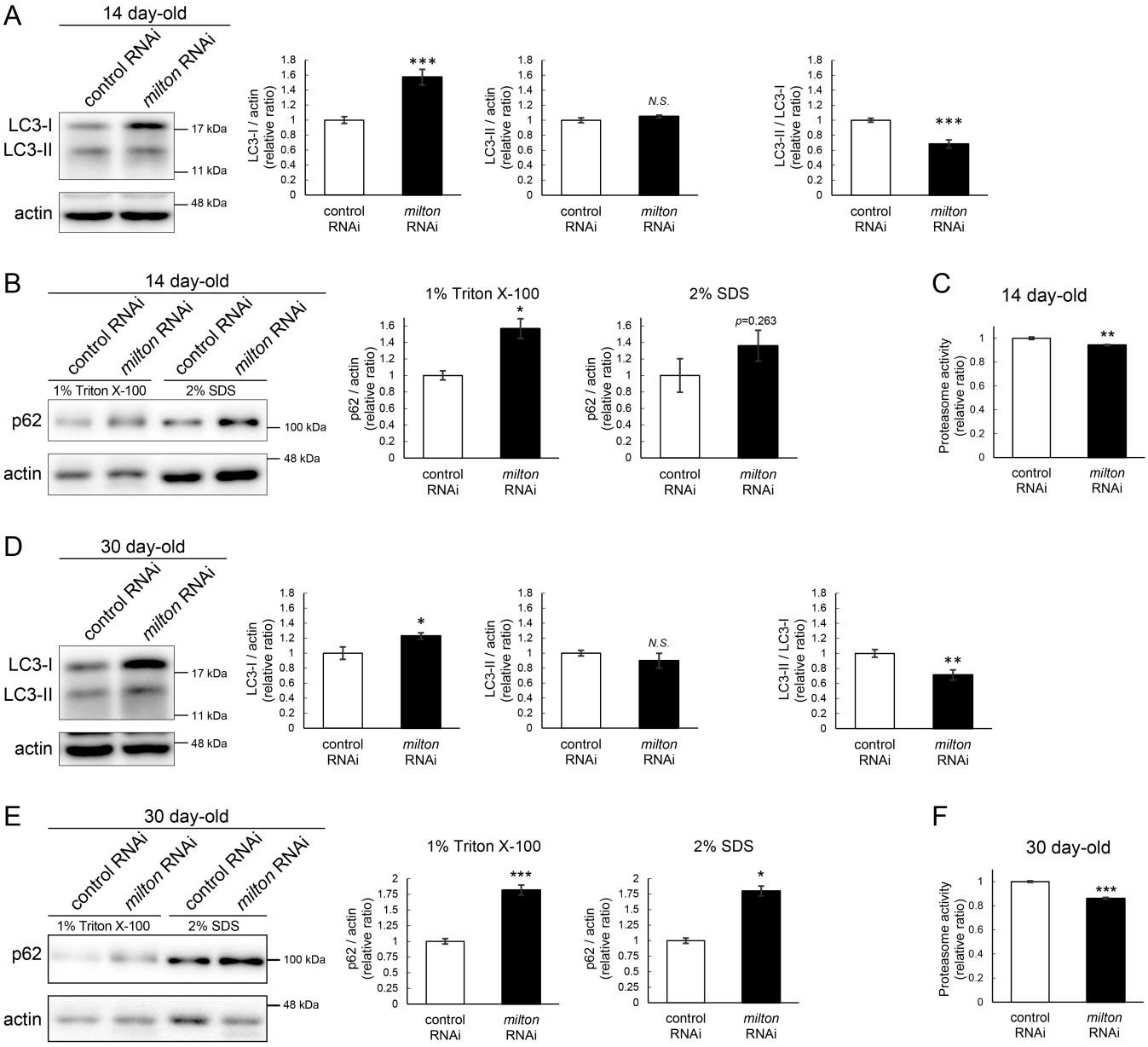

Shinno et. al., Figure 3

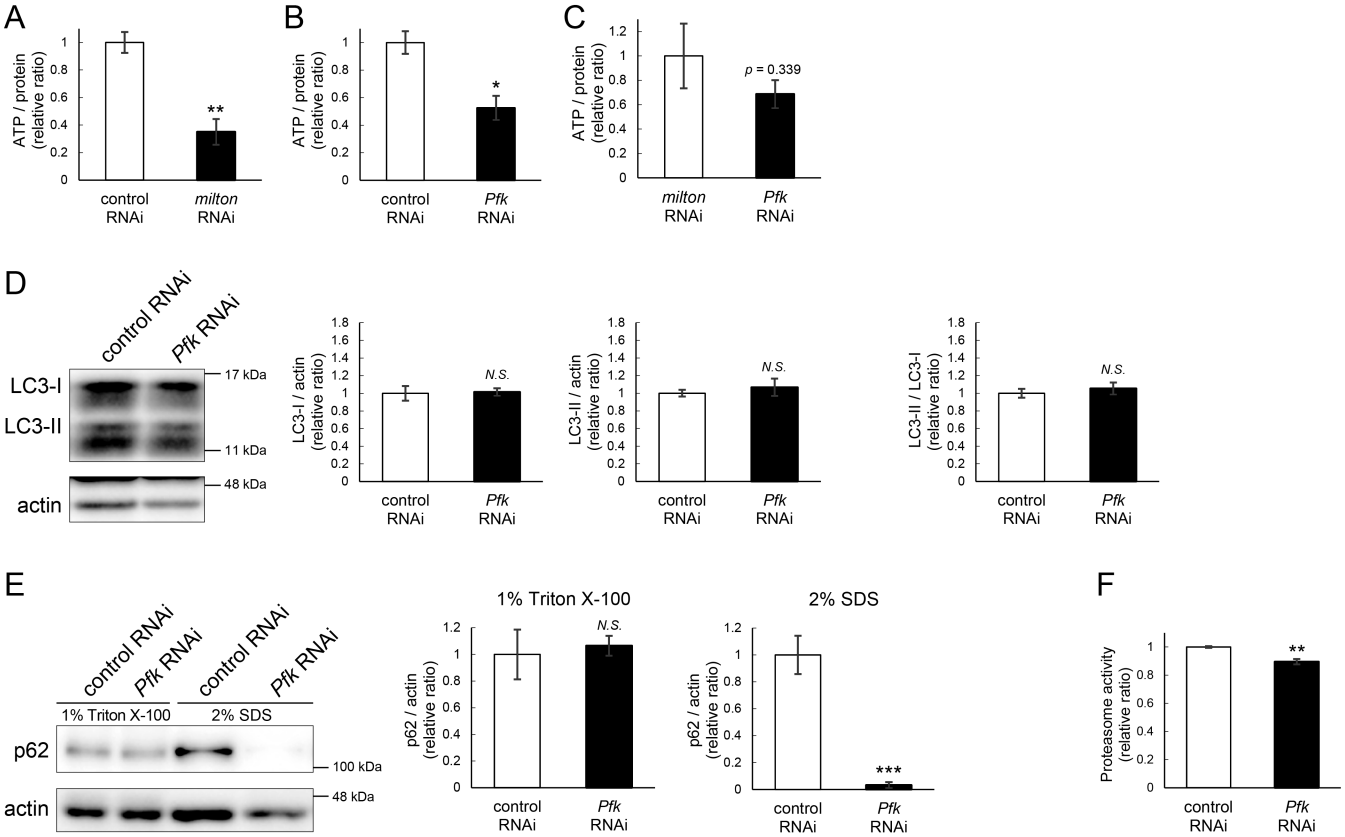

Shinno et. al., Figure 4

A

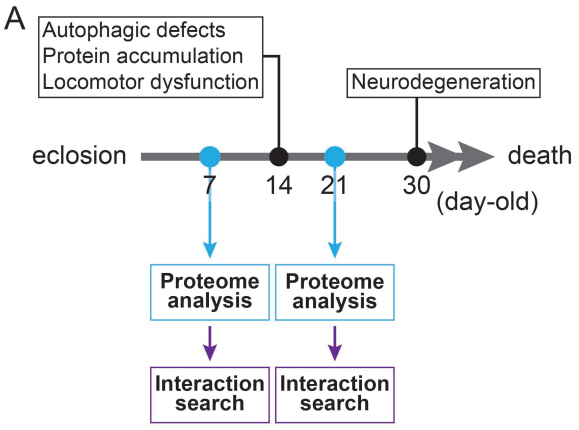

B

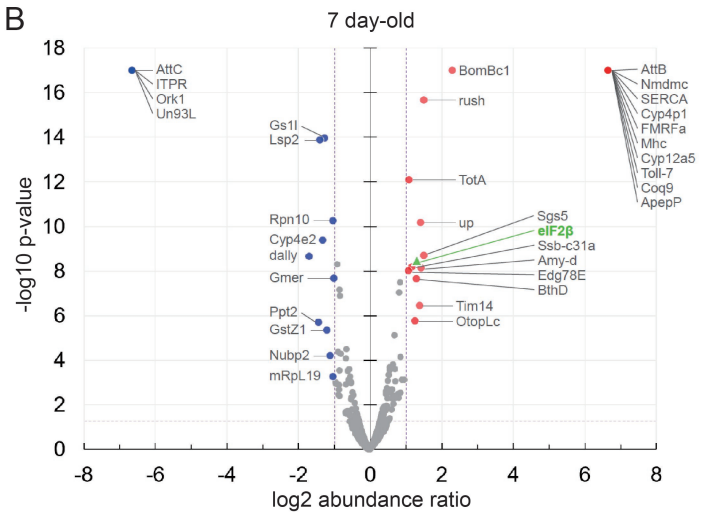

C

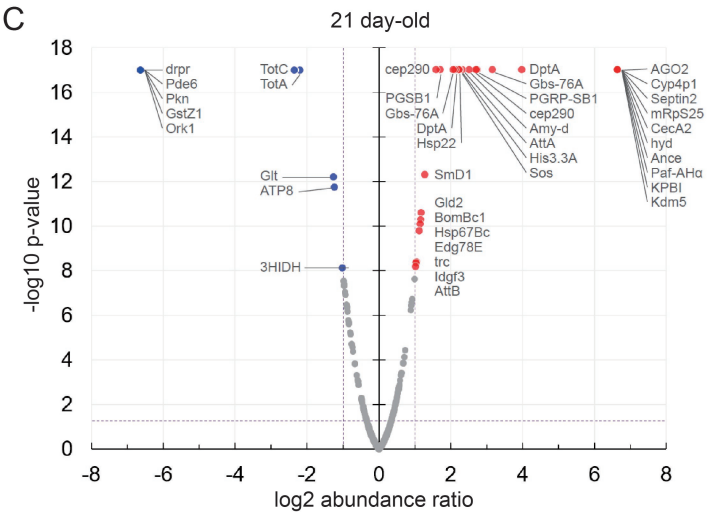

D

	Accession	Abundance Ratio : *milton* RNAi / control RNAi	
		7 day-old	21 day-old
eIF2α	P41374	1.106	0.961
eIF2β	P41375	2.465***	0.753*
eIF2γ	Q24208	0.952	0.952

E

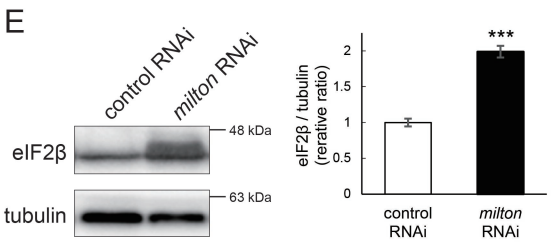

F

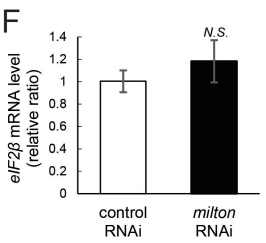

G

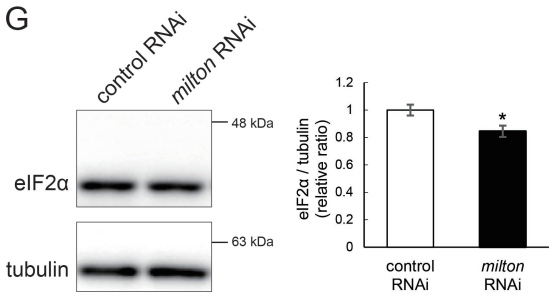

H

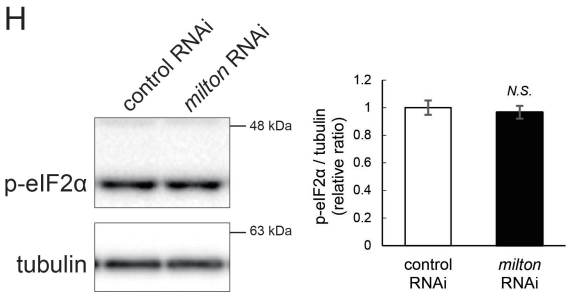

I

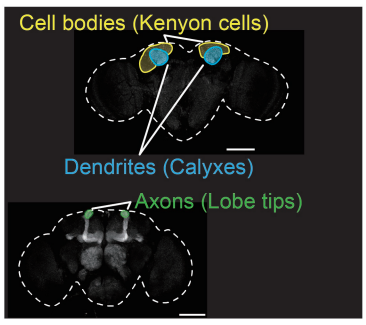

J

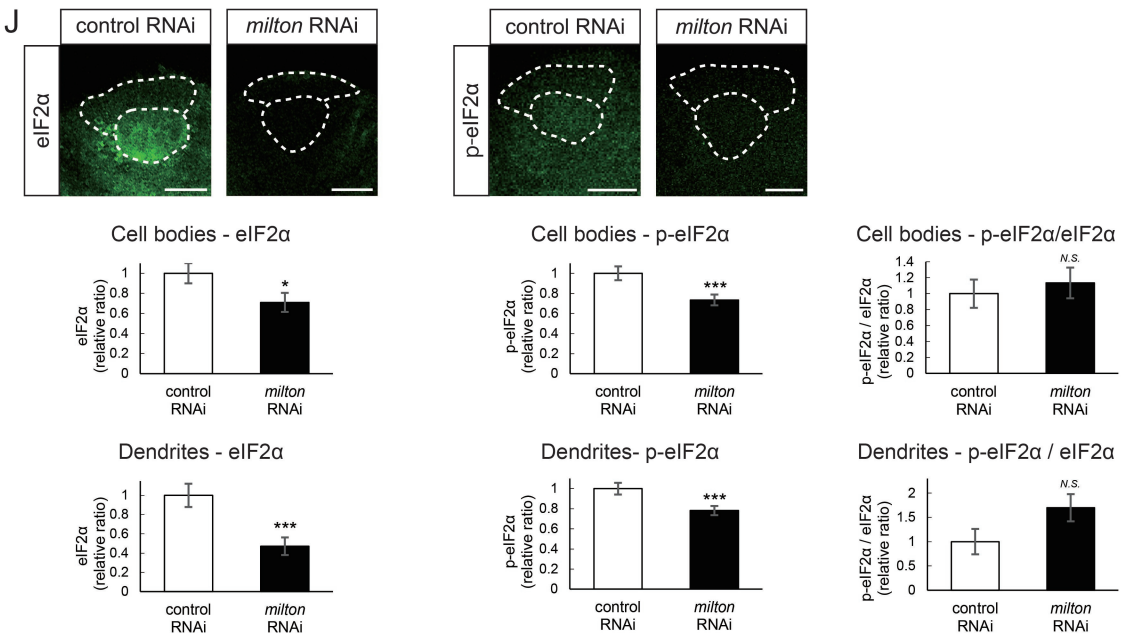

K

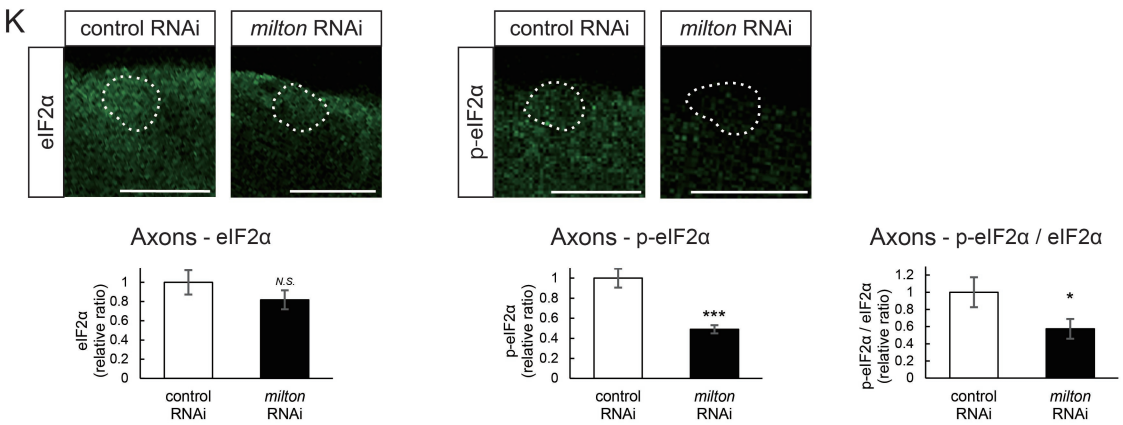

Shinno et. al., Figure 5

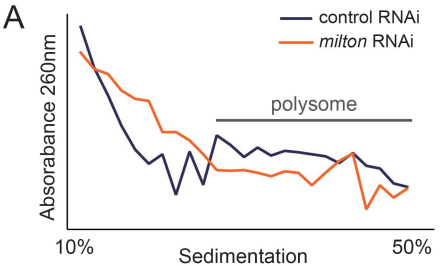

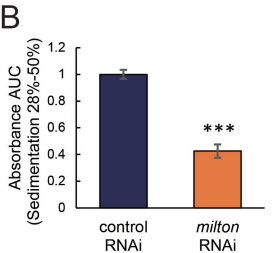

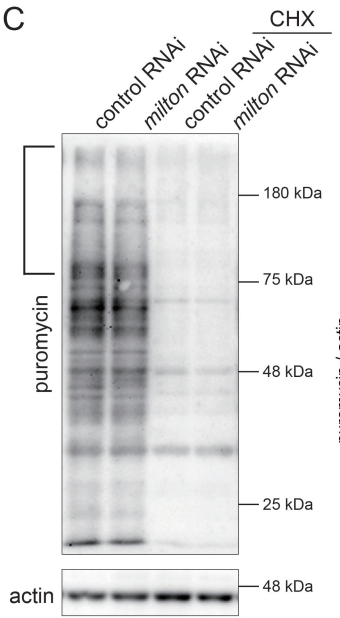

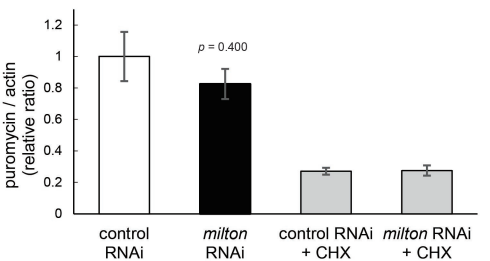

Shinno et. al., Figure 6

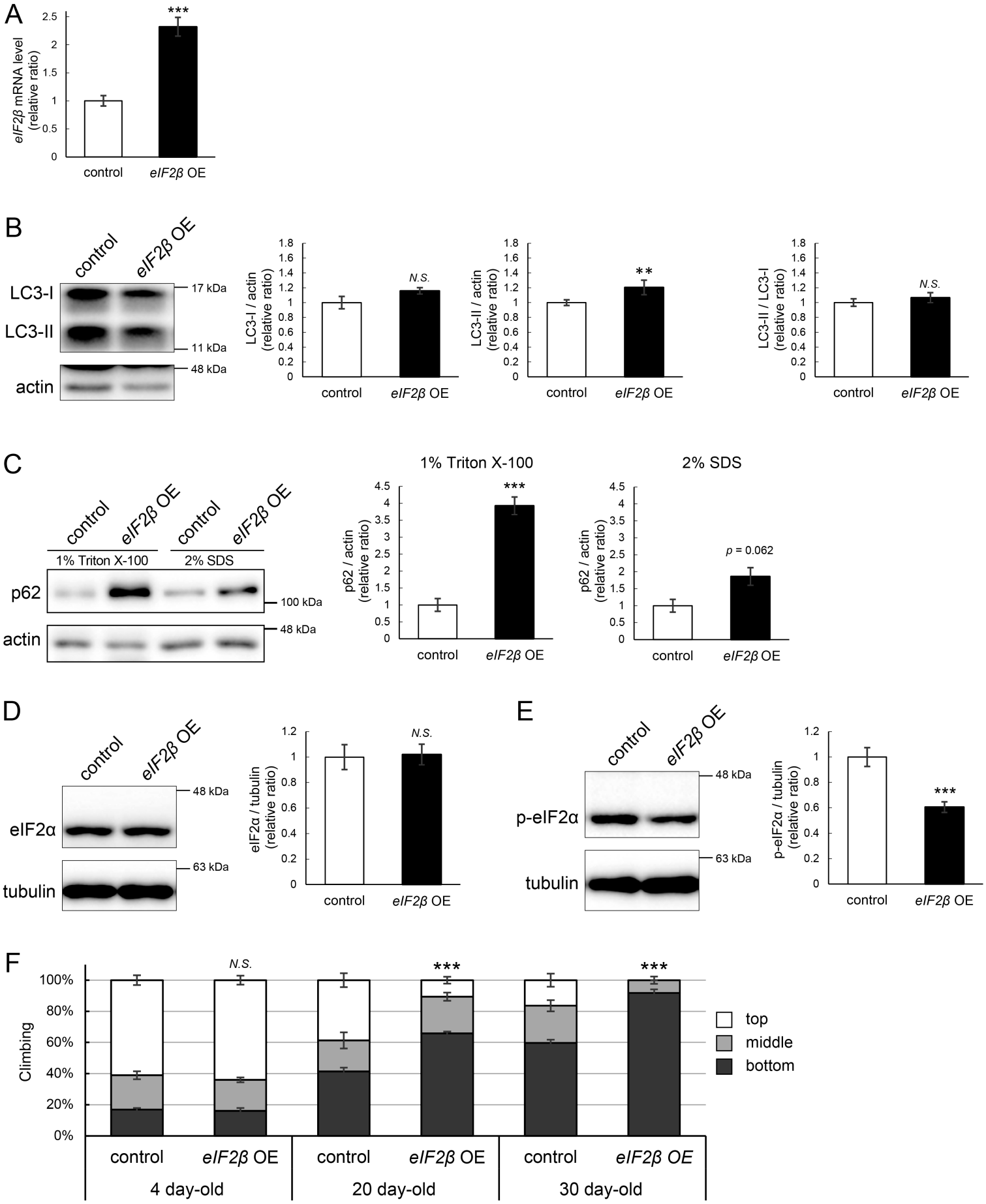

Shinno et. al., Figure 7

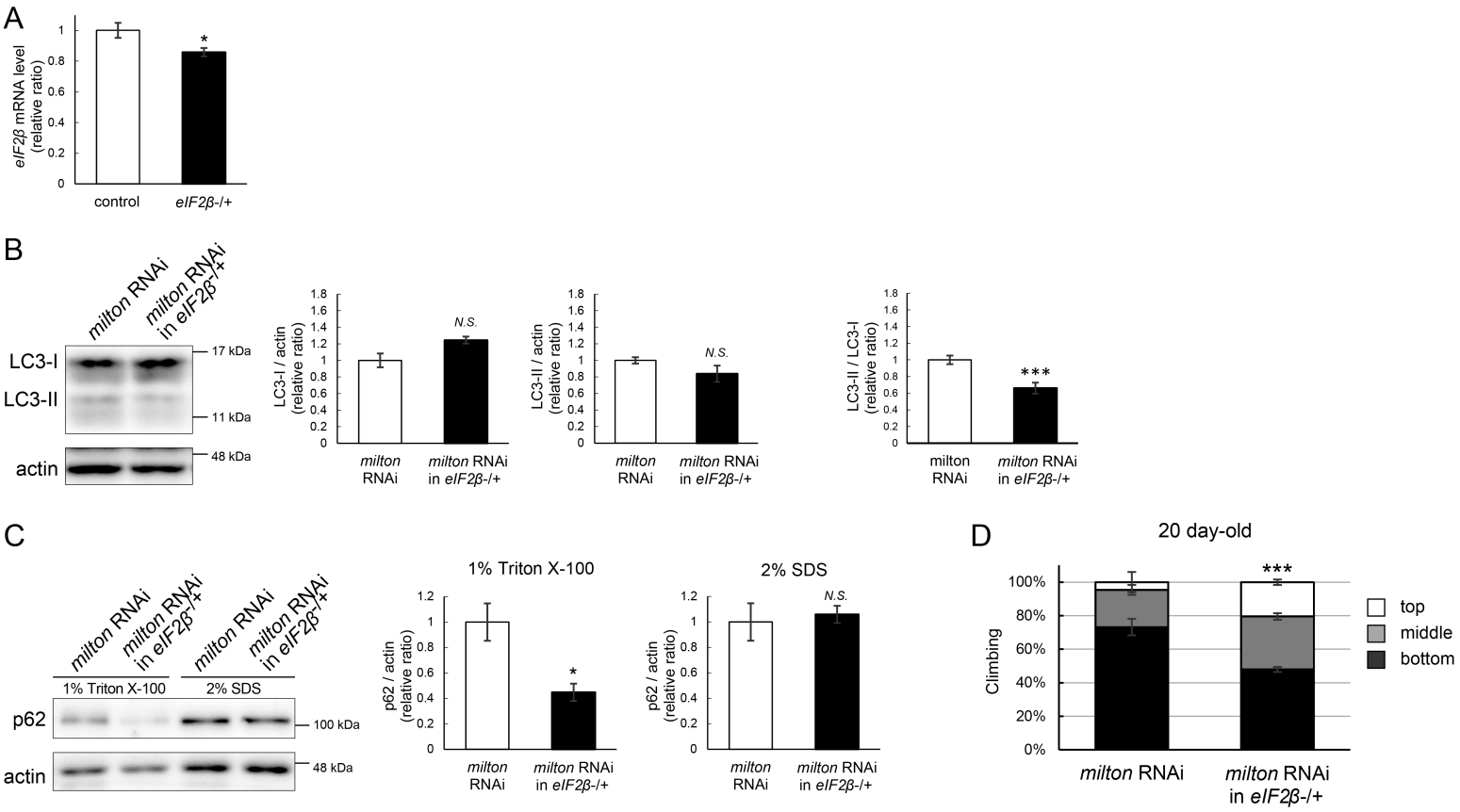

Shinno et. al., Figure 8

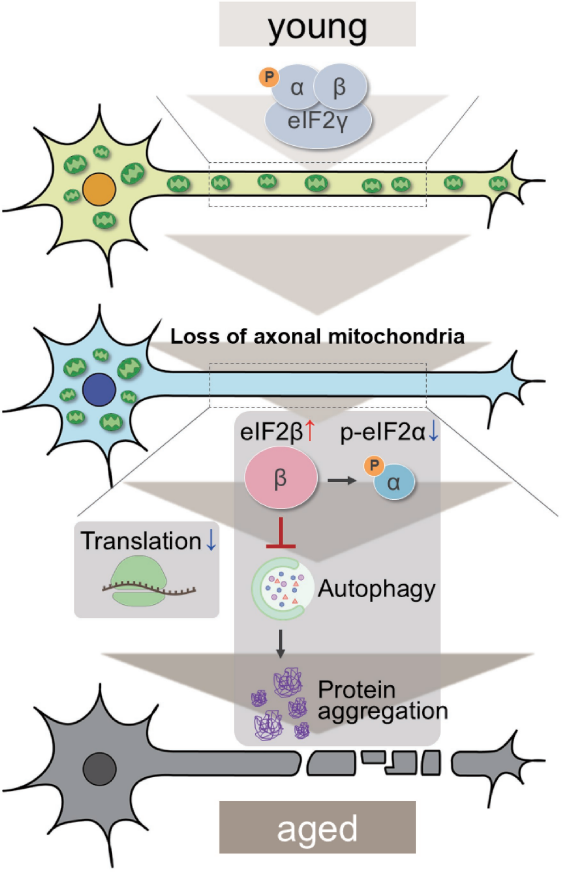

7 day-old			
Accession[a]	Name	Abundance Ratio: (7 days, milton KD) / (7 days, control)	Abundance Ratio P-Value: (7 days, milton KD) / (7 days, control)
Q9V751	Attacin-B	100	1E-17
Q04448	Bifunctional methylenetetrahydrofolate dehydrogenase/cyclohydrolase, mitochondrial	100	1E-17
P22700	Calcium-transporting ATPase sarcoplasmic/endoplasmic reticulum type	100	1E-17
Q9V558	Cytochrome P450 4p1	100	1E-17
P10552	FMRFamide-related peptides	100	1E-17
P05661-19	Isoform F of Myosin heavy chain, muscle	100	1E-17
Q9VE01	Probable cytochrome P450 12a5, mitochondrial	100	1E-17
Q7KIN0	Toll-like receptor 7	100	1E-17
Q8MKN0	Ubiquinone biosynthesis protein COQ9, mitochondrial	100	1E-17
Q9VJG0	Xaa-Pro aminopeptidase ApepP	100	1E-17
Q9V8F5	Bomanin Bicipital 1	4.908	1E-17
P07701	Salivary glue protein Sgs-5	2.843	1.99252E-09
Q76902	Pleckstrin homology domain-containing family F member 1 homolog	2.836	2.22045E-16
P81641	Alpha-amylase B	2.684	7.44847E-09
P19351-4	Isoform 4 of Troponin T, skeletal muscle	2.66	6.65563E-11
Q9VTJ8	Mitochondrial import inner membrane translocase subunit TIM14	2.61	3.54205E-07
P41375	Eukaryotic translation initiation factor 2 subunit 2	2.465	3.38486E-09
Q9VYB0	Selenoprotein BthD	2.462	2.25579E-08
B7Z0W9	Proton channel OtopLc	2.382	1.71741E-06
Q9VLR5	RNA polymerase II transcriptional coactivator	2.245	6.70245E-09
Q8IN44	Protein Turandot A	2.127	8.38662E-13
P27779	Pupal cuticle protein Edg-78E	2.113	1.00215E-08
Q9W1X8	Probable GDP-L-fucose synthase	0.496	2.12601E-08
P55035	26S proteasome non-ATPase regulatory subunit 4	0.487	5.50158E-11
Q9VHN6	39S ribosomal protein L19, mitochondrial	0.487	0.000551337
Q9VPD2	Cytosolic Fe-S cluster assembly factor NUBP2 homolog	0.46	6.34514E-05
Q9VHD3	Probable maleylacetoacetate isomerase 1	0.432	4.50956E-06
Q94529	Probable pseudouridine-5'-phosphatase	0.416	1.08802E-14
Q27606	Cytochrome P450 4e2	0.398	4.13128E-10
Q24388	Larval serum protein 2	0.378	1.33227E-14
Q9VKH6	Lysosomal thioesterase PPT2 homolog	0.369	2.05225E-06
Q24114	Division abnormally delayed protein	0.307	2.24406E-09
Q95NH6	Attacin-C	0.01	1E-17
P29993	Inositol 1,4,5-trisphosphate receptor	0.01	1E-17
Q94526	Open rectifier potassium channel protein 1	0.01	1E-17
Q9Y115	UNC93-like protein	0.01	1E-17

[a] UniProt accession number

21 day-old			
Accession[a]	Name	Abundance Ratio: (21 days, Milton KD) / (21 days, Control)	Abundance Ratio P-Value: (21 days, Milton KD) / (21 days, Control)
Q10714	Angiotensin-converting enzyme	100	1E-17
C0HKQ8	Cecropin-A2	100	1E-17
Q9V558	Cytochrome P450 4p1	100	1E-17
P51592	E3 ubiquitin-protein ligase hyd	100	1E-17
Q9VMJ7	Lysine-specific demethylase lid	100	1E-17
Q9VXP4	Platelet-activating factor acetylhydrolase IB subunit beta homolog	100	1E-17
Q9VY28	Probable 28S ribosomal protein S25, mitochondrial	100	1E-17
Q9W391	Probable phosphorylase b kinase regulatory subunit alpha	100	1E-17
Q9VUQ5	Protein argonaute-2	100	1E-17
P54359	Septin-2	100	1E-17
P24492	Diptericin A	15.716	1E-17
Q9VVY3	Glycogen-binding subunit 76A	8.986	1E-17
Q70PY2	Peptidoglycan-recognition protein SB1	6.669	1E-17
Q9W0M1	Centrosomal protein cep290	6.526	1E-17
P81641	Alpha-amylase B	5.722	1E-17
P45884	Attacin-A	4.997	1E-17
C0HL66	Histone H3.3A	4.778	1E-17
P26675	Protein son of sevenless	4.696	1E-17
P02515	Heat shock protein 22	4.69	1E-17
Q95NH6	Attacin-C	4.35	1E-17
P17971-1	Isoform A of Potassium voltage-gated channel protein Shal	4.195	1E-17
Q7K1U0	Activity-regulated cytoskeleton associated protein 1	3.271	1E-17
P14199	Protein ref(2)P	3.014	1E-17
Q9VU02	Probable small nuclear ribonucleoprotein Sm D1	2.43	4.91607E-13
Q9VD44	Poly(A) RNA polymerase gld-2 homolog A	2.268	2.6084E-11
Q9V8F5	Bomanin Bicipital 1	2.24	5.16671E-11
P22979	Heat shock protein 67B3	2.223	7.90048E-11
P27779	Pupal cuticle protein Edg-78E	2.192	1.65944E-10
Q9NBK5	Serine/threonine-protein kinase tricornered	2.059	4.15071E-09
Q8MLZ7	Chitinase-like protein Idgf3	2.055	4.61182E-09
Q9V751	Attacin-B	2.038	6.79416E-09
Q9V8M5	Probable 3-hydroxyisobutyrate dehydrogenase, mitochondrial	0.492	7.42952E-09
P84345	ATP synthase protein 8	0.421	1.809E-12
P33438	Glutactin	0.414	6.13731E-13
Q8IN44	Protein Turandot A	0.218	1E-17
Q8IN43	Protein Turandot C	0.195	1E-17
Q9VFI9	cGMP-specific 3',5'-cyclic phosphodiesterase	0.01	1E-17
Q94526	Open rectifier potassium channel protein 1	0.01	1E-17
Q9VHD3	Probable maleylacetoacetate isomerase 1	0.01	1E-17
Q9W0A0	Protein draper	0.01	1E-17
A1Z7T0	Serine/threonine-protein kinase N	0.01	1E-17

7 day-old					
Rank	Name	Score	Score (p) [a]	Score (v) [b]	Score (c) [c]
1	Autophagy-related protein signaling pathway	50.394	6.76E-16	0.159	0.11
2	Calcium signaling pathway	47.583	4.75E-15	0.146	0.117
3	Transcriptional regulation by SMAD	44.012	5.64E-14	0.146	0.095
4	GABA signaling pathway	40.706	5.58E-13	0.122	0.123
5	estrogen signaling pathway	37.507	5.12E-12	0.11	0.13
6	Sirtuin signaling pathway	36.87	7.96E-12	0.122	0.095
7	Transcriptional regulation by AP-1	34.874	3.18E-11	0.11	0.107
8	Arrestin signaling pathway	32.84	1.30E-10	0.11	0.092
9	G protein (Gq/11) signaling pathway	30.889	5.03E-10	0.085	0.149
10	Kainate receptor signaling pathway	30.049	9.00E-10	0.073	0.214
11	Transcriptional regulation by C/EBP	29.5	1.32E-09	0.098	0.093
12	Calpain signaling pathway	28.597	2.46E-09	0.11	0.066
13	Phospholipase D signaling pathway	28.344	2.94E-09	0.098	0.084
14	HSP90 signaling pathway	27.188	6.54E-09	0.085	0.104
14	CYP family	27.188	6.54E-09	0.085	0.104
16	Kir3 channel signaling pathway	26.495	1.06E-08	0.061	0.25
17	Estrogen biosynthesis	26.107	1.38E-08	0.061	0.238
18	CaSR signaling pathway	25.39	2.27E-08	0.061	0.217
19	PI3K signaling pathway	24.927	3.14E-08	0.073	0.122
20	PAF receptor signaling pathway	24.555	4.06E-08	0.049	0.4
21	Transcriptional regulation by PPARa	24.398	4.52E-08	0.073	0.115
21	BTK signaling pathway	24.398	4.52E-08	0.073	0.115
23	Transcriptional regulation by STAT	24.076	5.66E-08	0.085	0.077
24	G protein (Gi/o) signaling pathway	24.063	5.71E-08	0.073	0.111
25	PARP signaling pathway	23.742	7.13E-08	0.073	0.107
25	mGluR signaling pathway	23.742	7.13E-08	0.073	0.107
27	Free fatty acid signaling pathway	23.433	8.83E-08	0.073	0.103
28	Kir channel signaling pathway	23.338	9.43E-08	0.061	0.167
29	Oxytocin signaling pathway	23.327	9.51E-08	0.049	0.333
30	Transcriptional regulation by MEF2	22.99	1.20E-07	0.073	0.098
31	S100 family signaling pathway	22.434	1.77E-07	0.073	0.092
32	Transcriptional regulation by FOXO	22.301	1.94E-07	0.073	0.091
33	P2Y signaling pathway	22.172	2.12E-07	0.061	0.143
34	Transcriptional regulation by SRF	21.174	4.23E-07	0.061	0.125
34	ATF4/ATF6/IRE1 signaling pathway	21.174	4.23E-07	0.061	0.125
36	Chemerin signaling pathway	21.082	4.50E-07	0.049	0.235
36	Vasopressin signaling pathway	21.082	4.50E-07	0.049	0.235
38	Serotonin signaling pathway	20.854	5.28E-07	0.073	0.077
39	Transcriptional regulation by HIF	20.834	5.35E-07	0.098	0.043
40	Leukotriene receptorsignaling pathway	20.724	5.78E-07	0.049	0.222
40	CART signaling pathway	20.724	5.78E-07	0.049	0.222
42	MAPK signaling pathway	20.693	5.90E-07	0.085	0.055
43	Transcriptional regulation by RB/E2F	20.543	6.55E-07	0.098	0.042
44	NAD metabolism	20.468	6.89E-07	0.061	0.114
45	ERK signaling pathway	20.425	7.11E-07	0.073	0.073
46	Adenylyl Cyclase signaling pathway	20.303	7.73E-07	0.061	0.111
47	Bile acid signaling pathway	20.141	8.65E-07	0.061	0.109

[a] Score(p) indicates p-value of the pathway.
[b] Score(v) indicates the ratio of "Count" to total molecules associated with the loaded list.
[c] Score(c) indicates the ratio of "Count" to total molecules contained in the pathway.

21 day-old					
Rank	Name	Score	Score (p) [a]	Score (v) [b]	Score (c) [c]
1	Histone demethylation	84.198	4.51E-26	0.102	0.425
2	CDK inhibitor signaling pathway	56.497	9.83E-18	0.078	0.295
3	Transcriptional regulation by RB/E2F	46.598	9.39E-15	0.108	0.095
4	Mst(Hippo) signaling pathway)	46.343	1.12E-14	0.09	0.133
5	Transcriptional regulation by androgen receptor	46.078	1.35E-14	0.078	0.178
6	p160 SRC signaling pathway	45.809	1.62E-14	0.078	0.176
7	Transcriptional regulation by SMAD	43.961	5.84E-14	0.09	0.119
8	Autophagy-related protein signaling pathway	41.063	4.35E-13	0.084	0.119
9	Transcriptional regulation by HIF	39.527	1.26E-12	0.096	0.086
10	Nucleophosmin signaling pathway	38.417	2.72E-12	0.054	0.273
11	HSP90 signaling pathway	37.887	3.93E-12	0.066	0.164
12	PAF metabolism	37.562	4.93E-12	0.042	0.5
13	Transcriptional regulation by STAT	37.276	6.01E-12	0.072	0.132
14	Bcl-2 family signaling pathway	36.157	1.31E-11	0.072	0.124
15	Sirtuin signaling pathway	34.782	3.39E-11	0.072	0.114
16	Transcriptional regulation by C/EBP	33.819	6.60E-11	0.066	0.128
17	PIN1 signaling pathway	33.172	1.03E-10	0.06	0.149
18	RSK signaling pathway	30.566	6.29E-10	0.06	0.125
19	Transcriptional regulation by High mobility group protein	29.873	1.02E-09	0.054	0.148
20	BET family signaling pathway	29.656	1.18E-09	0.054	0.145
21	Transcriptional regulation by Myc	28.838	2.08E-09	0.066	0.093
22	Transcriptional regulation by FOXO	28.827	2.10E-09	0.054	0.136
23	PSD-95 family signaling pathway	26.154	1.34E-08	0.048	0.14
24	AKT signaling pathway	25.169	2.65E-08	0.048	0.129
25	Arginine methylation	24.799	3.43E-08	0.048	0.125
26	gp130 signaling pathway	24.25	5.01E-08	0.054	0.096
27	Transcriptional regulation by CREB	23.858	6.58E-08	0.066	0.067
28	Gene regulation by microRNAs (metastasis)	23.852	6.60E-08	0.054	0.093
29	HDAC signaling pathway	23.536	8.22E-08	0.036	0.207
30	Calpain signaling pathway	23.092	1.12E-07	0.06	0.074
31	Transcriptional regulation by IRF	22.738	1.43E-07	0.054	0.085
32	2-Oxoglutarate signaling pathway	22.673	1.50E-07	0.048	0.104
32	14-3-3 signaling pathway	22.673	1.50E-07	0.048	0.104
34	Transcriptional regulation by POU domain factor	22.601	1.57E-07	0.06	0.071
35	Transcriptional regulation by BLIMP-1	22.474	1.72E-07	0.042	0.132
36	Gene regulation by microRNAs (metabolism)	22.39	1.82E-07	0.054	0.083
37	Fatty acid beta oxidation	22.096	2.23E-07	0.042	0.127
38	Transcriptional regulation by RXR	22.08	2.26E-07	0.036	0.176
39	ERK signaling pathway	21.96	2.45E-07	0.048	0.098
40	PARP signaling pathway	21.913	2.53E-07	0.042	0.125
41	Transcriptional regulation by VDR	21.618	3.11E-07	0.054	0.078
42	Transcriptional regulation by p53	21.168	4.24E-07	0.072	0.05
43	Acetylcholine metabolism	21.152	4.29E-07	0.024	0.444
44	Gene regulation by microRNAs (embryonic stem cells)	21.08	4.51E-07	0.036	0.158
45	mTOR signaling pathway	21.048	4.61E-07	0.042	0.115
46	Gene regulation by microRNAs (cancer)	21.04	4.64E-07	0.048	0.09
47	Transcriptional regulation by Ets-1/2	20.724	5.77E-07	0.042	0.111
48	MAPK signaling pathway	20.411	7.18E-07	0.054	0.07
49	Gene regulation by microRNAs (cell cycle)	20.404	7.21E-07	0.036	0.146
50	Transcriptional regulation by p73	20.259	7.97E-07	0.042	0.106